Hygroscopicity and CCN potential of DMS derived aerosol particles

Bernadette Rosati[1,2], Sini Isokäntä[3], Sigurd Christiansen[1,4,5], Mads Mørk Jensen[1], Shamjad P. Moosakutty[1,6], Robin Wollesen de Jonge[1,7], Andreas Massling[8], Marianne Glasius[1], Jonas Elm[1], Annele Virtanen[3], and Merete Bilde[1]

[1]Department of Chemistry, Aarhus University, Denmark
[2]Faculty of Physics, University of Vienna, Austria
[3]Department of Applied Physics, University of Eastern Finland, Finland
[4]Faculty of Science and Technology, University of the Faroe Islands, Faroe Islands
[5]Department of Environmental Science, Stockholm University, Sweden
[6]Qatar Environment and Energy Research Institute, Hamad Bin Khalifa University, Qatar Foundation, Doha, Qatar
[7]Division of Nuclear Physics, Lund University, Sweden
[8]Department of Environmental Science, Aarhus University, Denmark

Correspondence: Bernadette Rosati (bernadette.rosati@chem.au.dk); Merete Bilde (bilde@chem.au.dk)

Abstract. Dimethyl sulphide (DMS) is emitted by phytoplankton species in the oceans and constitutes the largest source of naturally emitted sulphur to the atmosphere. The climate impact of secondary particles, formed through the oxidation of DMS by hydroxyl radicals, is still elusive. This study investigates the hygroscopicity and cloud condensation nuclei activity of such particles and discusses the results in relation to their chemical composition. We show that mean hygroscopicity parameters, κ, during an experiment for particles of 80 nm in diameter range from 0.46 to 0.52 as measured at both sub- and supersaturated water vapour conditions. Ageing of the particles leads to an increase in κ from for example 0.50 - 0.58 over the course of 3 hours (Exp. 7). Aerosol mass spectrometer measurements from this study indicate that this change most probably stems from a change in chemical composition leading to slightly higher fractions of ammonium sulphate compared to methanesulfonic acid (MSA) within the particles with ageing time. Lowering the temperature to 258 K increases κ slightly, particularly for small particles. These κ-values are well comparable to previously reported model values for MSA or mixtures between MSA and ammonium sulphate. Particle nucleation and growth rates suggest a clear temperature dependence, with slower rates at cold temperatures. Quantum chemical calculations show that gas-phase MSA clusters are predominantly not hydrated even at high humidity conditions indicating that their gas-phase chemistry should be independent of relative humidity.

1 Introduction

Aerosols originating from marine environments have a large impact on climate and are present over large parts of the Earth as oceans cover more than 70% of the Earths' surface (Seinfeld and Pandis, 2016). Marine aerosols affect climate not only by scattering and absorbing solar radiation, but also by acting as cloud condensation nuclei, CCN (e.g. IPCC, 2021). Marine aerosols consist of primary particles, mostly sea salt (Lewis and Schwartz, 2004) with various organic compounds (e.g. Facchini et al., 2008; Prather et al., 2013), and secondary particles comprising non-sea-salt sulphate originating from dimethyl sulphide (DMS) oxidation. DMS is emitted to the atmosphere due to the decomposition of dimethyl sulfoniopropionate, which in turn,

is produced by phytoplankton in the oceans (Andreae, 1990). In addition, exposure of corals to air has also been found to result in emission of significant amounts of DMS into the atmosphere (Hopkins et al., 2016). DMS is considered as one of the most abundant natural sulphur compounds in the atmosphere (e.g. Seinfeld and Pandis, 2016), and the global flux to the atmosphere is estimated to be $\sim$28 TgS each year (Carpenter et al., 2012). In the atmosphere DMS reacts primarily with hydroxyl radicals (OH) by either addition or hydrogen abstraction, where the relative importance of these two pathways has been shown to be sensitive to the prevalent temperature (Albu et al., 2006; Barnes et al., 2006). This reaction finally leads to compounds such as sulphuric acid (H_2SO_4, SA) and methanesulfonic acid (CH_3SO_3H, MSA) often found in the particle phase (Barnes et al., 2006; Mardyukov and Schreiner, 2018) as well as hydroperoxymethyl thioformate ($HOOCH_2SCHO$, HPMTF) (Veres et al., 2020; Ye et al., 2021).

Research on the importance of DMS for climate was stimulated by the so-called CLAW hypothesis (Charlson et al., 1987). The CLAW hypothesis proposes that higher ambient temperatures may increase the DMS production, which in turn, could enhance the formation of sulphate aerosol capable of acting as CCN. Subsequently, this could lead to changes in cloud micro-physical properties, coverage and lifetime, and therefore, cooling of the atmosphere. Although this hypothesis has been widely disputed, it has resulted in substantial progress in understanding the role of DMS oxidation products in the marine atmosphere (e.g. Ayers and Cainey, 2007; Vallina and Simó, 2007; Smith, 2007; Quinn and Bates, 2011).

Hoffmann et al. (2016) investigated the multi-phase chemistry of DMS by advanced box-models and presented a new parametrization to include important aqueous-phase chemical processes. They showed that the atmospheric conversion of DMS into MSA is highly underestimated if the aqueous-phase chemistry of DMS is not considered. Their revised set of oxidation mechanisms was essential to explain MSA ratios found in atmospheric aerosols. Recently, the secondary aerosol formation from DMS oxidation by hydroxyl radicals was studied in smog chamber experiments accompanied by kinetic multi-layer modelling (Rosati et al., 2021a; Wollesen de Jonge et al., 2021). It was observed that the secondary aerosol particle mass production from DMS oxidation was lower in experiments at humid conditions (relative humidity >50%) compared to dry ones (relative humidity <12%) for otherwise similar conditions of temperature, DMS and oxidant levels. In both cases the formed aerosol particles were found to consist mostly of MSA. Modelling and experimental data could be reconciled by including the newest parametrizations for DMS oxidation extended by revised and complete multi-phase DMS oxidation mechanisms (Wollesen de Jonge et al., 2021).

Despite the significant contribution of DMS to atmospheric aerosols, knowledge about key properties especially concerning the hygroscopicity and CCN activity of DMS derived aerosols are sparse. Hygroscopicity, which describes the ability of a particle to take up water at subsaturated water vapour conditions, is one key aspect of the climatic effects of aerosols, and it is predominately determined by the chemical composition of the particles. The CCN activity describes the potential of aerosol particles to be activated into cloud droplets at supersaturated water vapour conditions and it is known to depend on particle size and chemical composition (IPCC, 2021; Seinfeld and Pandis, 2016). The hygroscopicity (e.g. Berg et al., 1998; Nilsson et al., 2001; Lewis and Schwartz, 2004; Swietlicki et al., 2008; Modini et al., 2010; Fuentes et al., 2011) and ability to serve as CCN (e.g. Covert et al., 1998; Ovadnevaite et al., 2011; King et al., 2012; Prather et al., 2013; Collins et al., 2013, 2016; Nguyen et al., 2017; Fossum et al., 2018; Rosati et al., 2021b) of marine aerosols and sea spray aerosol in particular has been

studied intensively. Few studies have addressed the water uptake behaviour of secondary DMS derived aerosols. Methanesulfonate (MSA) particles were scrutinised in a few studies: Johnson et al. (2004) reported experimentally derived hygroscopic growth factors (GF) for MSA at high humidity conditions, obtaining GF(90%) = 1.57 for particles with a dry diameter of 100 nm. Tang et al. (2019) investigated various particulate methanesulfonates and obtained hygroscopicity parameters in the range of 0.37-0.47 based on CCN activity measurements (diameter: 40 - 60 nm) finding calcium methanesulfonate as the least and potassium and sodium methanesulfonate as the most hygroscopic compounds. The water cycle of sodium methanesulfonate, among others, have also been studied with an electrodynamic balance finding that particles deliquesce (i.e. dissolve completely) at RH=65.2-68.9 % and exhibit a GF(90%)=1.80 (Peng and Chan, 2001). Fossum et al. (2018) included the methanesulfonate anion to the list of ions considered in the Aerosol Inorganic-Organic Mixtures Functional groups Activity Coefficients (AIOM-FAC) model (Zuend et al., 2008, 2011) to predict the CCN activity of methanesulfonate particles including MSA, sodium and ammonium methanesulfonate. Their calculations suggest that MSA and sodium methanesulfonate activate at similar critical supersaturations while higher supersaturations are needed to activate ammonium methanesulfonate particles of the same size.

To our knowledge the hygroscopicity and CCN activity of complex aerosols formed in the oxidation of DMS have not been addressed before. Therefore, the aim of this study is to investigate comprehensively the hygroscopic growth and CCN activity of DMS-derived aerosols generated in an atmospheric simulation chamber and discuss these properties in relation to the chemical composition of the aerosols. Additionally, we show results of nucleation and growth rates of new particles formed through the oxidation of DMS with OH radicals. The experiments were designed to mimic a realistic marine atmosphere by simulating different relevant humidity and temperature conditions. For completeness, we also include in this work results from five experiments already presented by Rosati et al. (2021a) and/or Wollesen de Jonge et al. (2021) but not discussed with respect to hygroscopicity and CCN activation potential previously. Our extensive measurement setup covers the formation rates of particles larger than 1.7 nm, the growth rates of 10-20 nm particles, the water uptake of particles from 10-150 nm (dry size), and provides insight into the bulk chemical composition of the DMS derived aerosols. Experiments were additionally complemented by quantum chemical modelling of MSA clusters.

2 Methodology

2.1 Theory

2.1.1 Nucleation rate calculations

Particle nucleation rates were obtained using the method described in Tomicic et al. (2018). By measuring the concentration of particles with diameters exceeding a cut-off diameter of 1.7 nm ($N_{1.7}$), the nucleation rate $J_{1.7}$ is defined as:

$$J_{1.7} = \frac{dN}{dt} \qquad , N = \frac{N_{1.7}}{exp(-kt)} \tag{1}$$

where k denotes the rate of particle wall loss and t the time after the initiation of new particle formation. The cut-off diameter of 1.7 nm was selected according to Kulmala et al. (2013) being described as the critical cluster size from where nucleation

occurs and thus $J_{1.7}$ constitutes an approximation of the nucleation rate. $J_{1.7}$ was obtained from the wall-loss corrected particle number concentrations, calculating the gradient between 20 % and 80 % of the maximum particle number concentration.

2.1.2 Water uptake by atmospheric aerosols

90 The water uptake behaviour of aerosol particles at sub- and supersaturated conditions can be described by the Köhler equation:

$$S = a_w \cdot exp\left(\frac{4M_w\sigma_s}{RT\rho_w D(RH)}\right), \tag{2}$$

where S is the water vapour saturation ratio, a_w the water activity, σ_s the surface tension of the solution, R the ideal gas constant, T the absolute temperature, ρ_w the density of water, M_w the molecular mass of water and D(RH) the diameter of a

95 particle exposed to a certain relative humidity, RH.

At sub-saturated conditions of water vapour the hygroscopic growth factor at a given relative humidity (GF(RH) is calculated as the ratio of the particle diameter at high RH (D(RH)) to the dry particle diameter (D_{dry}):

$$GF(RH) = \frac{D(RH)}{D_{dry}}. \tag{3}$$

At supersaturated conditions of water vapour the critical supersaturation (SS_{crit}) needed for a specific particle size to be acti-

100 vated into a cloud droplet is in focus. This point is identified as the maximum of the Köhler curve (SS versus D(RH)).

To compare water uptake at sub- and supersaturated conditions, the hygroscopicity parameter κ, introduced by Petters and Kreidenweis (2007), can be used. The water activity term in Eq. 2 can then be described in terms of κ in the following way:

$$\frac{1}{a_w} = 1 + \kappa\frac{V_s}{V_w}, \tag{4}$$

where V_s is the volume of the dry particle and V_w the volume of the water in the droplet. By combining Eq. 2, 3 and 4 the

105 semi-empirical κ-Köhler equation can be obtained:

$$S = \frac{GF(RH)^3 - 1}{GF(RH)^3 - (1 - \kappa)} \cdot exp\left(\frac{4M_w\sigma_s}{RT\rho_w D(RH)}\right). \tag{5}$$

For a given supersaturation (or RH for the subsaturated case) a κ_{GF} and $\kappa_{SS_{crit}}$ can be calculated.

2.2 Experimental Procedure

Experiments were carried out at the Aarhus University Research on Aerosol (AURA) atmospheric simulation chamber (Kris-

110 tensen et al., 2017). In short, the facility consists of a 5 m^3 Teflon bag situated inside a temperature controlled room allowing experiments to be performed in the temperature range 257 to 299 K. The chamber is equipped with 24 UV lamps (wavelengths: 300-400 nm) located at the top and bottom of the bag. In high humidity experiments a custom-built humidifier was used to increase the relative humidity in the chamber to RH=70 %. H_2O_2 (30 % in H_2O, Merck, 1.07209.0250) was evaporated from

a heated round-bottom flask (at 403 K) and flushed into the chamber using heated N_2 (333-343 K, 10 L/min). By photolysing

115 H_2O_2, OH radicals were produced. The OH radical concentrations in the experiments are estimated to be in the range of typical tropospheric concentrations (4.64-5.71E+06 molecules cm^{-3}; Seinfeld and Pandis, 2016) based on supplementary experiments investigating the decay of 1-butanol in the bag (Rosati et al., 2021a, b; Wollesen de Jonge et al., 2021). Either 200 or 400 ppb of DMS (Sigma Aldrich, anhydrous ≥99.0 %, 274380) were injected into the chamber by evaporating a known amount and guiding it into the chamber using 10 L min^{-1} of N_2 gas heated to 333 K. The sequential order of the procedure was: 1) setting

120 the desired chamber temperature, 2) filling the chamber with purified air (Active Carbon, HEPA filter and zero-air generator (Aadco Model 737-14)), 3) injecting humidified air to reach the desired RH, 4) injecting H_2O_2, 5) switching the UV lights on, 6) injecting DMS. The injection of DMS denotes the "time-0" in the experiments. Ammonia concentrations during the experiments are estimated to be between 1-10 ppb based on data from Tange (56.352222°N, 9.5875°W; ∼50 km from Aarhus; http://ebas.nilu.no/). Table 1 presents an overview of the experimental conditions. All instruments were operated at the labora-

125 tory temperature of 22°C outside the AURA chamber. To limit evaporation in tubing en route to the particle size (SMPS) and chemical composition measurement (AMS), the tubing was insulated. Particle size distributions and chemical composition for Exp. 5 and 9 were already presented in Wollesen de Jonge et al. (2021). This work focuses on the water uptake of the studied aerosol particles, thus Exp. 1, 5, 6, 7 and 9 are presented in terms of the hygroscopicity and CCN activity, which were not addressed in any of the previous studies (Rosati et al., 2021a; Wollesen de Jonge et al., 2021).

Table 1. Experimental conditions. T_{ch} and RH_{ch} denote the mean measured temperature and RH together with their standard deviations (1 sd) in the chamber. The DMS concentrations indicate the measured concentrations after injection except in Exp. 3, 6 and 7 marked with an asterisk where theoretical values are given based on the liquid injected into the chamber as the PTR-ToF-MS was not available. Additionally, NO_x concentration ranges, H_2O_2 mixing ratios and particle growth rates (GR) obtained for the size range 10-20 nm are listed. Lower H_2O_2 mixing ratios correspond to injections of 418 μL, while higher ones to 1500 μL. See also Rosati et al. (2021a) for additional information regarding Exp. 1, 6, and 7 and Wollesen de Jonge et al. (2021) for experiments 5 and 9. The last column specifies if any data of these experiments were previously presented.

Exp. number	Date	RH_{ch} [%]	T_{ch} [K]	DMS [ppb]	NO_x [ppb]	H_2O_2 [ppm] *	GR [nm h^{-1}]	
1	13.02.2019	5.2 ± 0.2	292.6 ± 0.1	120	0-11.6	65.6	13.1 ± 0.6	see also Rosati et al. (2021a)
2	15.02.2019	63.0 ± 5.5	292.4 ± 0.4	150	0-2.3	65.6	24.8 ± 3.8	
3	05.03.2019	62.2 ± 1.2	292.8 ± 0.3	200*	0-1.4	235.5	20.2 ± 0.5	
4	22.02.2019	58.5 ± 1.8	292.4 ± 0.4	310	0-1.5	65.6	20.5 ± 0.9	
5	26.02.2019	56.4 ± 4.4	292.4 ± 0.4	330	0-1.0	235.5	26.2 ± 1.9	see also Wollesen de Jonge et al. (2021)
6	04.03.2019	13.7 ± 1.7	292.8 ± 0.1	400*	0-9.7	235.5	15.9 ± 1.1	see also Rosati et al. (2021a)
7	07.03.2019	9.2 ± 0.6	292.8 ± 0.2	400*	0-20.1	235.5	15.5 ± 0.5	see also Rosati et al. (2021a)
8	18.02.2019	73.2 ± 5.7	273.2 ± 0.8	170	0-1.4	61.2	16.3 ± 0.7	
9	01.03.2019	75.5 ± 4.1	273.1 ± 0.8	220	0-0.3	219.5	11.9 ± 0.4	see also Wollesen de Jonge et al. (2021)
10	20.02.2019	70.7 ± 5.1	259.3 ± 1.3	120	0-3.1	57.8	4.5 ± 0.0	
11	28.02.2019	75.3 ± 1.0	258.8 ± 0.2	280	0-0.7	207.4	7.7 ± 0.9	

*Mixing ratios calculated assuming a smog chamber volume of 5 m^5 and a density of the H_2O_2 solution (30% in H_2O) of 1.11 g ml^{-1}.

2.3 Instrumentation and Analysis

2.3.1 Stationary instrumentation

Nitrogen oxides (NO_x) and ozone (O_3) levels were continuously measured with a chemiluminescent monitor (AC32M, Environnement S.A) and a UV absorption ozone analyser (O342 Module, Environment S.A), respectively. The temperature (T) and RH were monitored in the centre of the bag (HC02-04 sensor; Rotronic AG, Switzerland).

2.3.2 Volatile organic compounds

During Exp. 1, 2, 4, 5 and 8-11 a Proton Transfer Reaction Time-of-Flight Mass Spectrometer (PTR-ToF-MS 4000, Ionicon Analytik, Innsbruck, Austria; e.g. Graus et al., 2010; Cappellin et al., 2012; Sekimoto et al., 2017) was employed to continuously monitor DMS concentrations. The instrument is based on a soft-ionisation technique using hydronium ions (H_3O^+) to ionise gas-phase compounds with proton affinities equal to or greater than that of water, which is the case for most volatile organic compounds (VOC). After the reaction with the primary ion occurs in the drift tube, the ionised compounds are detected in the ToF-MS. The PTR-ToF-MS was run with drift tube conditions of 650 V, 80°C and 2.4 mbar and thus an E/N number of 143 Townsend. The instrument was connected to the chamber via a 2 m long Teflon tube, wrapped in heating tape set to 60°C, that was connected to the heated inlet of the instrument (temperature set to 80°C). Additionally, the instrument flow rate was increased by adding a sheath flow of 200 mL min^{-1} to reduce sampling losses.

Data analysis was performed using the PTR-MS Viewer 3 (Ionicon). Prior to the measurement campaign a transmission calibration was carried out based on specific reaction rate constants and mass discrimination factors as described elsewhere (Taipale et al., 2008; Liu et al., 2018).

2.3.3 Particle number concentration

An Airmodus A11 nano Condensation Nucleus Counter (nCNC, Airmodus), consisting of a Particle Size Magnifier (PSM, Airmodus A10) and a Condensation Particle Counter (CPC, Airmodus A20), was used to measure particles above 1.7 nm in diameter during Exp. 5, 9 and 11. A thorough description of the instrument is given elsewhere (Vanhanen et al., 2011). In short, the PSM was operated with diethylene glycol as working fluid. Supersaturated diethylene glycol leads to growth of the smallest (approximately 1 nm) particles by condensing the working fluid onto them. When the particles reach sizes of approximately 90 nm they are guided to a condensation particle counter (using butanol as working fluid) and optically detected therein. The PSM was operated in fixed mode, counting all particles above the selected 1.7 nm threshold. The saturator flow rate was kept at 0.28 L min^{-1} in order to obtain the desired cut-off diameter.

2.3.4 Particle size distributions

A Scanning Mobility Particle Sizer (SMPS, TSI model 3938) was used to measure the dry particle number size distributions. The Electrostatic Classifier (EC, TSI model 3082) was either connected to a nano Differential Mobility Analyser (DMA; TSI

model 3085A) for sizes between 2 and 65 nm or a long DMA (TSI model 3081) for the size range 10-422 nm. Initially the nano DMA was used and switched to the long DMA when particles grew out of the size range. The DMAs were connected to a nano Water-based Condensation Particle Counter (WCPC, TSI model 3788). The SMPS data analysis was performed with the Aerosol Instrument Manager (AIM) version 10.2.0.11 using the corrections for diffusion losses and multiple charges. A sheath to aerosol flow ratio of 10:1 was chosen (Nano SMPS: 15:1.5 L min^{-1}; Long SMPS: 6:0.6 L min^{-1}). A silica gel diffusion dryer was used to ensure a RH<10% at the inlet of the SMPS.

In order to retrieve particle properties, such as hygroscopicity, representative for the main particle mode, we used the size distributions measured with SMPS over time. A log-normal distribution was fitted to the SMPS data at every time step. The mean and standard deviation of the particle number size distribution were retrieved from the fit. A particle size was classified as representative for the major particle population in the chamber when it was within the fitted mean $\pm$ 1 sd of the SMPS size distribution. All mean values presented in the manuscript refer to the time when particle properties were measured within the main growth-mode. An example for the limits found for Exp. 5 is shown in Fig. S1 in the supplementary information (SI).

2.3.5 Water uptake at sub- and supersaturated conditions

The hygroscopic growth of 10-150 nm (dry size) particles was measured with two separate Humidified Tandem Differential Mobility Analysers (HTDMA) at a constant RH of 80 %. In brief, an HTDMA consists of two DMAs, a CPC and a humidifier in-between the two DMAs. The first DMA is used to select a monodisperse sample from the dry polydisperse particle population, which is then exposed to a selected RH. The size distribution of the humidified particles is then measured with the second DMA followed by the CPC. In this way the hygroscopic growth factor GF(RH) can be retrieved (Eq. 3). The hygroscopic growth of particles with D_{dry}=10, 15 and 20 nm particles was measured with a custom built "nano-HTDMA" described in more detail e.g. in Keskinen et al. (2011) and Tikkanen et al. (2018). In short, the nano-HTDMA system consists of two nano-DMAs (TSI, model 3085) and a water based CPC (TSI, model 3785) to count the particles. A silica gel diffusion drier was placed in front of the first DMA to make sure the particles entered the instrument with RH<10 %. The DMAs were operated in an open-loop system, with a sample flow of 1 L min^{-1} and a sheath flow of 10 L min^{-1}. To ensure stable conditions through the particle sizing, the sample flow and the sheath air inside the second DMA were humidified separately. The measured GFs were then corrected to the target RH of 80 % assuming a constant hygroscopicity parameter κ within small deviation around the target humidity ($\pm$1.5 %), as in Tikkanen et al. (2018). Ammonium sulphate particles (Sigma Aldrich, purity $\geq$99.0 %) were used to calibrate the instrument for offsets in dry size selection. After taking into account the uncertainties of all devices influencing particle sizing, the uncertainty in the GFs can be estimated to be at maximum 2.5 %. The hygroscopic growth of particles with D_{dry}=30, 50, 80, 100 and 150 nm was measured with a commercially available HTDMA (Brechtel, Model 3002, Lopez-Yglesias et al., 2014), from now on termed "long-HTDMA". A diffusion drier at the inlet ensured that particles entered the instrument at RH<10 %. The aerosol flow of the first and second DMA were 0.8 and 0.5 L min^{-1}, respectively, while the sheath flows were 5 L min^{-1} in both systems. The instrument was calibrated using ammonium sulphate (Sigma Aldrich, purity >99.95 %) particles. The overall uncertainty in GF(80 %) is estimated to be below 3 %, based on the combination of

instrumental uncertainty (estimated to be 2 % sizing accuracy and 1 % RH uncertainty) and comparison to theoretical values calculated with Köhler theory (max. 2 % for the chosen size range).

The ability of particles to act as cloud condensation nuclei (CCN) was monitored with a Continuous-Flow Streamwise Thermal-Gradient CCN Chamber (CFSTGC, CCN-100 from Droplet Measurement Technologies; Roberts and Nenes, 2005). The CCN instrument was operated following the Scanning Mobility CCN Analysis (SMCA) described in Moore et al. (2010) to increase the temporal resolution. In short, we measured the critical dry diameter, $D_{p,c}$ of mobility size-selected aerosols. Aerosol laden air from AURA was dried using diffusion dryers (RH<10 %), before entering the Electrostatic Classifier. The classifier consisted of a long-DMA (TSI model 3081) and an aerosol neutraliser (X-ray source, TSI model 3087). A scanning voltage was applied (scan time 120 s up and 15 s down) and the mono-disperse outlet stream of the DMA was directed to both the CCNc and CPC (TSI model 3010). Time was synchronised daily. The CCN supersaturation was initially set high ($\sim 1.4\%$), since the newly formed aerosols were small in the beginning. As the particle size distribution grew to larger sizes, the supersaturation of the CCNc was decreased to ~ 0.2 %, which is representative for supersaturations found in the marine environment (Ditas et al., 2012). Scan time alignment, multiple charge correction, quality control, sigmoidal fitting of the activation curves (CCN/CN vs. D_p) was done using the "SMCAProcessor.xls" file available at http://nenes.eas.gatech.edu/ Experiments/SMCA.html (Accessed February 2019). The supersaturation of the CCN column was calibrated on the 11.03.2019 using atomised ammonium sulphate (99.9999 % purity, 33 mg in 500 mL MilliQ). The measured $D_{p,c}$ was used as input to the "Köhler curves" module of the Extended AIM Aerosol Thermodynamics Model to estimate the supersaturation (http: //www.aim.env.uea.ac.uk/aim/kohler/kohler2.php, accessed March 2019). A schematic of the SMCA calibration setup and a calibration curve performed with ammonium sulphate are shown in Fig. S2 and Fig. S3 in the SI.

2.3.6 Chemical composition of particles

A High-Resolution Time-of-Flight Aerosol Mass Spectrometer (HR-ToF-AMS, Aerodyne Research Inc.) was used to measure the chemical composition of the particles in real time. The instrument setup is described in detail in Decarlo et al. (2006). The instrument was employed as described in Rosati et al. (2021a). HR-ToF-AMS data were processed in Igor Pro 8 by the data analysis software packages SQUIRREL (version 1.62) and PIKA (version 1.22). The PIKA default HR-ToF-AMS collection efficiency (CE) of 1 was used. The MSA calibration as presented in Rosati et al. (2021a) was applied to quantify particulate MSA. Unit-mass resolution efficient Particle Time-of-Flight (ePToF) data was exported for the MSA tracer ion *m/z* 79 and sulphate tracer ion *m/z* 80. This sulphate tracer ion was selected because MSA only contributes $0.04 \cdot [m/z\ 79]$ to the *m/z* 80 signal. The relationship between vacuum aerodynamic diameters as retrieved from ePToF data and mobility diameters for spherical particles, used in the measurement of the water uptake, can be calculated according to DeCarlo et al. (2004):

$$\rho_p = \frac{d_{va}}{d_m}\rho_0, \tag{6}$$

where d_{va} is the vacuum aerodynamic diameter, d_m is the electric mobility diameter, ρ_0 is standard density (1 g cm^{-3}) and ρ_p is the density of the particle. The particles were assumed to have no voids, which results in the density of the particle to be equal

225 to the density of the material. PToF time series were smoothed using a 15-point (i.e. 15 minutes) moving average to decrease short-term fluctuations.

2.4 Quantum Chemical Calculations

To obtain molecular level insight into the hydration free energy of MSA, we carried out highly accurate quantum chemical calculations of the MSA-hydrate cluster structures. These calculations will aid in elucidating to what extent the MSA molecules
230 are hydrated in the gas-phase.

2.4.1 Computational Details

The Gaussian09 (Frisch et al., 2013) program was used to obtain the molecular cluster structures and calculate the vibrational frequencies. The ωB97X-D (Chai and Head-Gordon, 2008) functional was employed as it has been shown to exhibit low errors in the binding energies of atmospheric molecular clusters compared to higher level CCSD(T) calculations (Leverentz et al.,
235 2013; Elm et al., 2013; Elm and Kristensen, 2017). The calculations were performed using the 6-31++G(d,p) basis set, which has shown good agreement with basis sets of significantly larger sizes (Elm and Mikkelsen, 2014; Myllys et al., 2016).

The ORCA program version 4.0.0 (Neese, 2012) was used to calculate the single point energy (i.e. the electronic energy of a molecule for a certain arrangement of the atoms in the molecule) of all the clusters using DLPNO-CCSD(T$_0$) (Riplinger and Neese, 2013; Riplinger et al., 2013) with an aug-cc-pVTZ basis set. The aug-cc-pVTZ/C and aug-cc-pVTZ/JK auxiliary basis
240 set were used for density fitting and Coulomb/exchange fitting. We have recently demonstrated that this level of theory yields total and relative binding energy results in good agreement with higher level explicitly correlated coupled cluster calculations on a test set of 45 cluster structures (Schmitz and Elm, 2020) and sulphuric acid hydrates (Kildgaard et al., 2018a). All the thermochemical parameters have been calculated at 298.15 K and 1 atm.

2.4.2 Cluster Structure Sampling

245 We have recently reported the application of a systematic sampling technique to obtain the molecular structures of sulphuric acid - water clusters (Kildgaard et al., 2018a) and carboxylic acid - water clusters (Kildgaard et al., 2018b). Here we utilise the same method to thoroughly sample the rich potential energy surface of the methanesulfonic acid (MSA) - water clusters. The following procedure was applied:

1. Water molecules are placed around all the exterior atoms of the cluster.

250 2. Generated conformers are optimised using the PM6 (Stewart, 2007) method.

3. Identical conformers were excluded based on energy and rotational temperature.

4. The Gibbs free energy is calculated at the ωB97X-D/6-31++G(d,p) level of theory.

5. All conformers below 3 kcal/mol are then used as input structures for the addition of the next water molecules (step 1).

This approach generates a massive amount of conformers (350, 1084, 2027, 6801 and 5542 for the respective hydrates) and will yield a qualified guess for the global minimum cluster structure.

3 Results and Discussion

3.1 Nucleation and Growth Rates at Different Temperatures

Figure 1a presents particle number concentrations and nucleation rates of particles larger than 1.7 nm in diameter at 258 K (in blue), 273 K (in orange) and 293 K (in red) measured during Exp. 5, 9 and 11, respectively. The highest particle number concentrations were recorded at 298 K, and the lowest ones at 258 K. Nucleation rates increased with increasing temperature, e.g. from 68.7 cm^{-3}s^{-1} at 258 K to 426.3 cm^{-3}s^{-1} at 293 K. New particle formation was initiated at an earlier point in time at 293 K (immediately after DMS injection) compared to 258 K (approximately 10 minutes after DMS injection).

Figure 1b shows particle growth rates (GR) of particles with diameters between 10 and 20 nm, calculated using the maximum-concentration method (Lehtinen and Kulmala, 2003; Kulmala et al., 2012). The overall GR range (4.5 - 26.2 nm h^{-1}; see values in Table 1) fits well with ambient values measured in marine and coastal areas (1.8 - 20 nm h^{-1}; Manninen et al., 2010; Yli-Juuti et al., 2011). Similar to the nucleation rates, GR increase with increasing temperature. The colour code in Fig. 1b denotes the RH during the experiments. Results at 293 K show that lower RH values lead to lower GR compared to experiments performed at high RH.
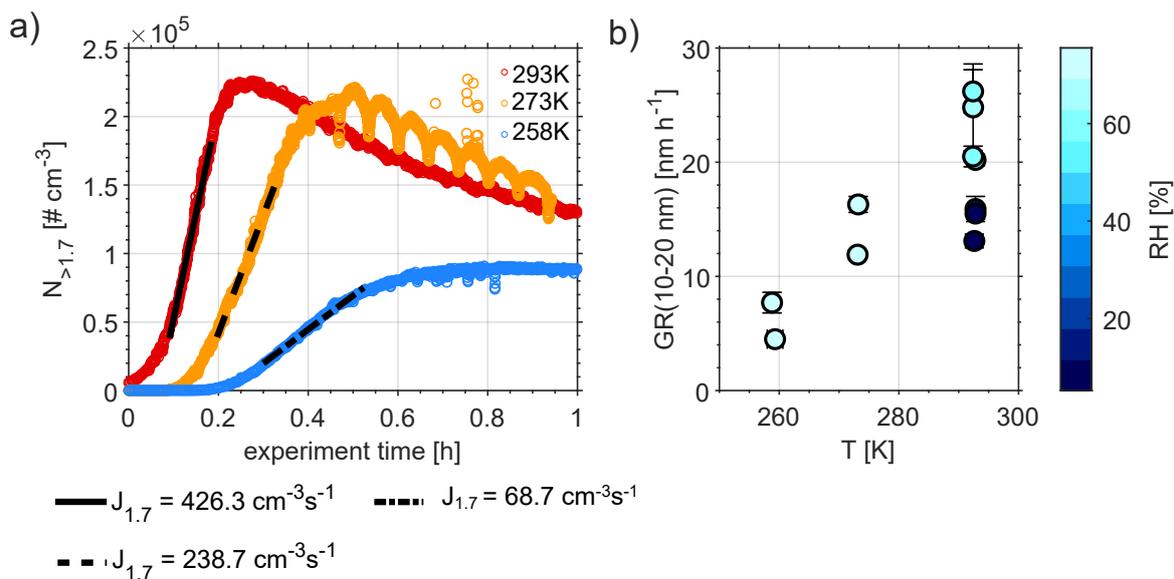
Figure 1. a) Nucleation rates (J) of particles larger than 1.7 nm during Exp. 5, 9 and 11 and b) growth rates (GR) for the size range from 10 to 20 nm at three different temperatures during Exp. 1-11. The fluctuations seen at T=273 K are due to the fact that the PSM was set to measure in scanning mode after a while.

The decrease of nucleation and growth rates with decreasing temperature is consistent with a lower observed loss rate of DMS at lower temperatures, see Fig. S4 and Table S1 in SI illustrating an example for each of the temperatures investigated in this study and a comparison between dry and humid experiments (Exp. 1, 2, 8 and 10). Different temperature trends for the rate of the reaction of DMS with OH radicals have been reported in the literature (Albu et al., 2006; Barnes et al., 2006; Hoffmann et al., 2016). Our observed trend is in line with the predicted temperature dependence obtained with the Arrhenius expression used in the Master Chemical Mechanism version 3.3.1 (MCMv3.3.1) and Hoffmann et al. (2016) delineating slower reaction rates at colder temperatures. The decay of the concentration of DMS over time for similar experiments at 293 and 273 K, dry and humid conditions, was formerly presented in Rosati et al. (2021b) and Wollesen de Jonge et al. (2021). Wollesen de Jonge et al. (2021) found good agreement between measured and modelled decay rates using the ADCHAM box model.

Nucleation and growth rates are known to be inherently dependent on temperature and RH (Seinfeld and Pandis, 2016). Typically at lower temperatures both nucleation and growth rates increase as the Gibbs free energy barrier decreases. This has also been observed in laboratory experiments with homogeneous nucleation of sulphuric acid and water at temperatures between 207 - 299 K and RH between 11 and 58 % (Duplissy et al., 2016). Ambient measurements of nucleation and growth rates, however, show ambiguous trends probably related to different temperature dependent processes occurring at the same time (Kerminen et al., 2018). A possible explanation for the decreasing nucleation and growth rates with decreasing temperatures seen in this study can be that the oxidation of DMS is slower at colder temperatures, thus fewer volatile compounds are available for cluster formation as they are formed more slowly. This is also supported by the above presented DMS decay trends illustrating slower decay rates with colder temperatures. The absolute water concentration could also have an effect on the observed trends in the nucleation rate as the initial cluster formation in our chamber setup most likely consist of relatively weakly bound sulphuric acid – methane sulfonic acid – ammonia clusters (Rosati et al., 2021a). Water has been shown to increase the nucleation rate if the initial cluster is weakly bound such as for sulphuric acid – ammonia clusters (Henschel et al., 2014b, 2016). However, in our studies the absolute concentration of water is lowest at colder temperatures.

OH concentrations in the chamber were obtained from the decay of 1-butanol due to reactions with OH radicals produced by photolysing H_2O_2. 1-butanol decay rates and resulting OH concentrations for experiments performed at the same temperature and humidity conditions as used in the herein presented DMS experiments are illustrated in Fig. S5 and Table S2 in the SI. The herein found OH concentrations are in the range of tropospheric levels (e.g. 1-2E+06 molecules cm^{-3} Seinfeld and Pandis, 2016; 1.09E+06 molecules cm^{-3} Li et al., 2018).

3.2 Hygroscopicity, CCN activity and Chemical Composition

3.2.1 Effect of Atmospheric Ageing at 293 K

Atmospheric ageing of DMS derived secondary aerosols was simulated by prolonged exposure to OH radicals at different temperatures and RH. We first consider the water uptake at sub- and supersaturated water vapour conditions at 293 K for both dry and humid conditions. Figure 2 illustrates the water uptake behaviour in the form of κ-values obtained from hygroscopic growth and CCN measurements overlaid on particle number size distributions during Exp. 5 (humid conditions) and Exp. 7 (dry

11

conditions). In both cases clear nucleation events are visible with particles growing up to approximately 150 nm in diameter within the first 10 hours. As mentioned in Rosati et al. (2021a) an additional growth mode is observed and from Fig. 2 it seems to be more pronounced at dry compared to humid conditions (Fig. 2a vs. b).

305 κ-values are only presented for times when the selected dry diameter was within the boundary chosen to represent the main growth mode (see description in Sect. 2.3.4). The colour code describes the magnitude of κ, where dark blue colours represent low values and light blue colours high values. Mean κ-values during the main particle growth mode for 80 nm particles (dry size) as retrieved from long-HTDMA measurements in Exp. 5 and 7 were κ=0.52 $\pm$ 0.03 and κ=0.54 $\pm$ 0.03, respectively. These were calculated from GF(80%) results of 1.42 $\pm$ 0.02 and 1.44 $\pm$ 0.02. κ-values derived for other particle sizes are

310 presented in Table 2, and the GF(80%) results are presented in Table S3 (SI). In comparison κ-values from CCNc measurements for dry particles of approximately 80 nm yielded κ=0.50 $\pm$ 0.03 and κ=0.54 $\pm$ 0.06, for Exp. 5 and 7 respectively (all mean κ-values from CCNc are presented in Table S4 in SI). Thus, for this size, mean κ-values at sub- and supersaturated water vapour conditions are well comparable and agree within the standard variations of the measurements. Figure S6 shows the derived mean κ-values as a function of all measured dry particle diameters for Exp. 5 and 7. There is no systematic trend in

315 variation of κ with particle diameter for κ-values calculated from GFs, while an increase in κ with particle size can be seen for κ values calculated from CCNc data. Such a size trend can be expected from Köhler theory; for comparison the κ-value for ammonium sulphate varies from 0.51 to 0.63 over the particle size range 20-100 nm (calculated using UManSysprop at 293 K, Topping et al., 2016). Mean κ-values during the main particle growth mode are consistent across instruments and supersaturations. Agreement between κ-values derived for the same particle size from measurements at sub- and supersaturation is

320 not necessarily expected as shown by several earlier studies for organic and inorganic particles (e.g. Petters and Kreidenweis, 2007; Whitehead et al., 2014; Pajunoja et al., 2015; Zhao et al., 2016; Rastak et al., 2017; Rosati et al., 2020).

Following the evolution of κ for a certain size in Fig. 2 it can be seen that the values increase over time meaning that hygroscopicity increases with ageing by exposure to OH radicals and UV light indicating slight changes in chemical composition. In Exp. 7, performed at dry conditions (Fig. 2a), dry 80 nm particles could first be measured approximately 4 hours after the

325 start of the experiment showing κ-values of 0.50, which increased to κ-values of 0.58 at about 7 hours after the start of the experiment. Similarly, in Exp. 5, performed at humid conditions (Fig. 2b), the κ-value for dry 80 nm particles changed from 0.51 to 0.63 (measured at approximately 4 and 8 hours after start of the experiment). Similar trends were observed in Exp. 8 and 10 performed at different temperatures and shown in SI.

To further investigate this change in hygroscopicity as a result of ageing, we extracted size-selected ePToF data from the

330 HR-ToF-AMS. Figure 3 illustrates the temporal evolution of *m/z* 79 and 80, representative for MSA and ammonium sulphate, respectively. Only data for particles with an aerodynamic diameter of approximately 126 nm are illustrated as these correspond to particles with a mobility diameter of 80 nm assuming that particles were spherical and composed of approximately 50 % MSA and 50 % ammonium sulphate thus having a density of approximately 1.6 g cm^{-3} (density of MSA: 1.48 g cm^{-3}, density of ammonium sulphate: 1.77 g cm^{-3}; according to Sigma-Aldrich). This assumption is based on bulk chemical composition

335 data from HR-ToF-AMS presented in Fig. S7 (SI). Only results for Exp. 5 (wet conditions) and Exp. 6 (dry conditions) are shown, as the signal on the chosen marker ions was highest during these experiments and thus best PToF data analysis could

12

be performed. The black lines in Fig. 3 denote the ratio of *m/z* 79 to 80 and the vertical grey, dashed lines depict the time interval when this selected size was present within the main particle growth mode. When performing a linear regression to the ratio of *m/z* 79 to 80 when the ion signal was above 0.2 (threshold chosen to be less influenced by noise) a slow decrease is

340 visible, indicating an increased fraction of ammonium sulphate in the particles with time (red solid lines in Fig. 3) under both dry and humid conditions. During this campaign the HR-ToF-AMS was not set-up in a way to resolve size-selected properties at low aerosol mass concentration as only 30 s were spent on ePToF data acquisition for each 1 min data point. Thus, these results have to be treated with care and further experiments targeting size-selected chemical composition of secondary particles formed from the oxidation of DMS are needed to obtain a more detailed understanding of changes in the chemical composition

345 of DMS derived products.

Previous HTDMA measurements of pure MSA-particles at 293 K yielded GF(90 %)=1.57 for a dry particle size of 100 nm (Johnson et al., 2004), which translates to κ=0.36 and GF(80 %)=1.33 (recalculated using κ-Köhler theory). Fossum et al. (2018) predicted the supersaturation needed to activate MSA particles at 293.15 K with dry sizes between 20 and 200 nm with the AIOMFAC model, finding a κ-value of 0.55 for 80 nm particles (critical supersaturations presented in SI of

350 Fossum et al. (2018) and recalculated using κ-Köhler theory). Lower κ-values of 0.40 for 80 nm particles were modelled for ammonium-MSA (Fossum et al., 2018). In comparison κ-values for 80 nm ammonium sulphate particles are 0.59 and 0.62 according to the UManSysProp thermodynamic model (Topping et al., 2016) for subsaturated (GF(80 nm,80 %)) and supersaturated (80 nm dry size) conditions, respectively. Assuming particles composed of 50% MSA and 50% ammonium
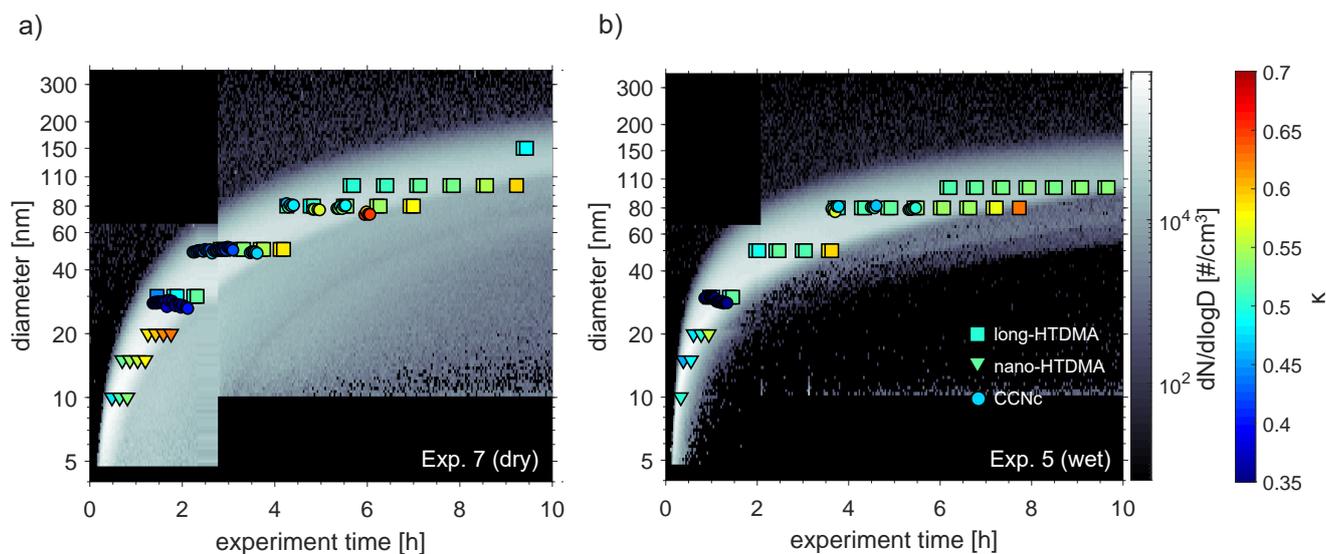
Figure 2. κ values as obtained from nano- (triangles), long-HTDMA (squares) CCNc (circle) measurements for different dry particle sizes. Particle number size distributions of the DMS derived aerosol particles at dry and wet conditions are shown in the background. Results are from a) Exp. 7 (dry) and b) Exp. 5 (wet).
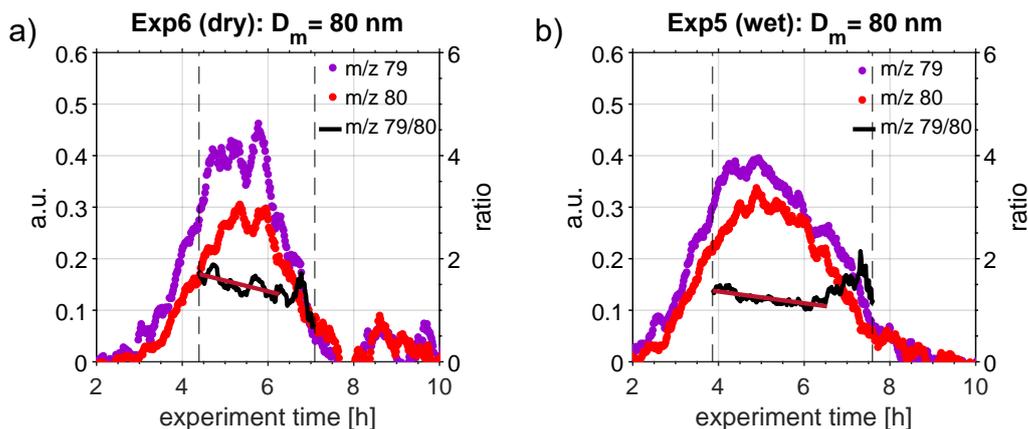
Figure 3. Temporal evolution of *m/z* 79 (violet dots) and 80 (red dots), representative for MSA and ammonium sulphate, respectively, as measured in the HR-ToF-AMS during a) Exp. 6 (dry conditions, T=293 K) and b) Exp. 5 (wet conditions, T=293 K). The black solid lines denote the ratio of *m/z* 79/80 as calculated during the main particle growth mode in the chamber (represented by vertical dashed lines). A linear fit was calculated for the ratio during the time period where both ions had a signal higher than 0.2 (dark red line), indicating a linear decrease over this period.

sulphate, as indicated by the HTR-ToF-MS results in this study, mixed κ-values can be retrieved using the modelled data of
355 the single substances yielding 0.57 and 0.59 for 80 nm particles using ammonium sulphate results at sub- and supersaturated conditions, respectively. Our mean κ results are considerably higher than those for pure MSA from HTDMA measurements presented earlier by Johnson et al. (2004) and closest to AIOMFAC κ-values for MSA while being lower than the ammonium sulphate values from UManSysProp. The range of κ-values measured within this study is consistent with the hygroscopicity of a mixture of MSA and ammonium sulphate. As the hygroscopicity of ammonium sulphate is larger than that of MSA, a change
360 in chemical composition during ageing leading to a higher fraction of ammonium sulphate in the particles could be responsible for the measured increase in hygroscopicity over time.

3.2.2 Effect of Lower Temperatures

Experiments at 258, 273 and 293 K and high relative humidity were carried out to explore how the hygroscopicity and CCN activation potential is affected by the temperature during particle formation and subsequent ageing. Similar to the results at
365 293 K, the hygroscopicity of the particles formed at 258 and 273 K increases with ageing (see Fig. S8 and S9 in SI). Figure 4a illustrates mean GF(80 %) as measured by nano- and long-HTDMA and Fig. 4b mean κ-values as calculated from HTDMA and CCNc results for the three different temperatures. The mean values are calculated from the time period when a certain size was measured in the main growth mode as described in Sect. 2.3.4. Only data for humid experiments are shown, i.e. Exp. 2-5 and 8-11. Table 2 shows mean κ-values for each experiment (mean GF(80 %) values and mean κ-values from the
370 CCNc are presented in Table S4 in the SI). When comparing results at 293 K in Fig. 4a, it is evident that GF(80 %) values

14

are smaller for smaller sizes. This difference disappears when κ-values are compared (spherical symbols), indicating that this difference originates from the Kelvin term that is more important for particles of approximately 15 nm in dry size compared to approximately 80 nm. GF(80%) values in the long-HTDMA range seem comparable at all temperatures, while the nano-HTDMA shows a tendency for smaller GF(80%) at 293 K compared to 258 K. When comparing HTDMA data in Fig. 4b illustrating κ-values, this general trend of less hygroscopic particles at 293 K compared to 258 K is also visible. Figure 4b additionally illustrates κ-values as derived from CCNc measurements (square symbols). Generally, the ranges of the CCNc results are more scattered but they overlap with HTDMA results. The majority of the herein presented experimental κ-values lie in the range of modelled values for MSA and ammonium-MSA as found by Fossum et al. (2018) (theoretical values depicted in Fig. 4b) and the experimental κ-values at 258 K for small particles exceed the modelled MSA results and are more comparable with the theoretical κ-values for ammonium sulphate.
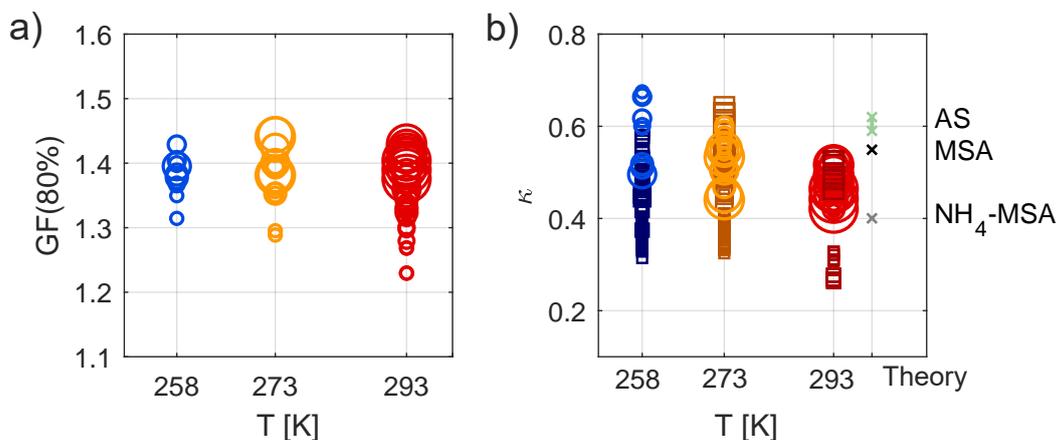
Figure 4. Temperature dependence of water uptake: a) GF(80 %) as measured from nano- and long-HTDMA (spheres), b) κ-values as measured from nano, long-HTDMA (spheres) and CCNc (squares). The size of the markers is related to the dry particle size selected, i.e. smaller markers describe results for smaller particles and vice versa. Results describe Exp. 2 - 5 and 8 - 11 at high humidity conditions. The theoretical κ values are taken from Fossum et al. (2018) for MSA and NH$_4$MSA for 80 nm dry particles and from the UManSysProp model for ammonium sulphate (AS) as found for 80 nm dry particles as recalculated from sub- and supersaturated water vapour conditions.
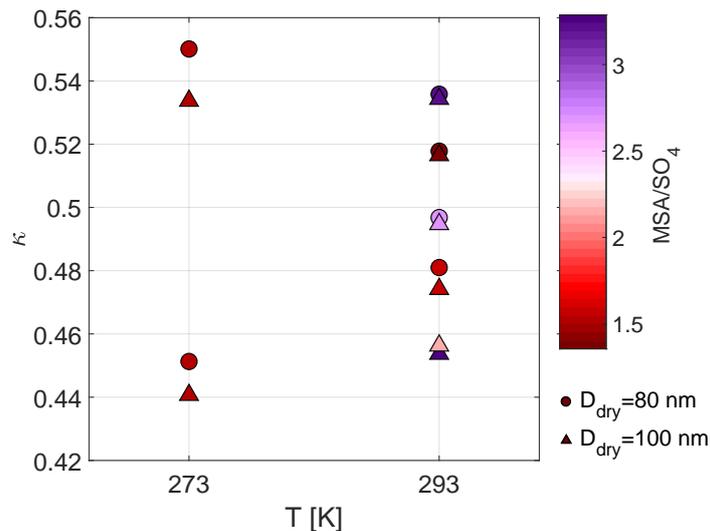
Figure 5. Mean κ-values at 273 K and 293 K for particles with dry sizes of 80 and 100 nm. Colour scheme shows the average MSA to sulphate ratio during the time period when the specific dry size was measured. Exp. 1-9 are shown.

Table 2. Mean κ-values and their standard deviations (1 sd) as calculated from nano- and long-HTDMA.

Exp. number	D_{dry} = 10 nm	D_{dry} = 15 nm	D_{dry} = 20 nm	D_{dry} = 30 nm	D_{dry} = 50 nm	D_{dry} = 80 nm	D_{dry} = 100 nm	D_{dry} = 150 nm
1	1.26 ± 0.00	1.30 ± 0.02	1.34 ± 0.02	1.36 ± 0.02	1.40 ± 0.02		1.39 ± 0.01	1.36 ± 0.00
2	1.23 ± 0.01	1.30 ± 0.01	1.34 ± 0.02	1.34 ± 0.04	1.36 ± 0.03		1.39 ± 0.01	1.38 ± 0.00
3	1.27 ± 0.01	1.30 ± 0.02	1.34 ± 0.01	1.32 ± 0.03	1.38 ± 0.02	1.40 ± 0.02	1.40 ± 0.01	
4	1.23	1.28 ± 0.02	1.32 ± 0.03	1.33 ± 0.04	1.38 ± 0.03	1.41 ± 0.02	1.42 ± 0.02	1.39 ± 0.01
5	1.27	1.30 ± 0.01	1.33 ± 0.01	1.35 ± 0.04	1.41 ± 0.03	1.42 ± 0.02	1.43 ± 0.02	1.40 ± 0.01
6	1.28 ± 0.01	1.34 ± 0.01	1.38 ± 0.01					
7	1.27 ± 0.01	1.34 ± 0.01	1.38 ± 0.02	1.36 ± 0.02	1.41 ± 0.03	1.44 ± 0.02	1.44 ± 0.02	1.44 ± 0.02
8	1.29 ± 0.02	1.36 ± 0.01	1.39 ± 0.01	1.35 ± 0.03	1.40 ± 0.02	1.38 ± 0.02	1.38 ± 0.01	
9	1.30 ± 0.00	1.35 ± 0.01	1.40 ± 0.01	1.39 ± 0.02	1.42 ± 0.00	1.44 ± 0.02	1.44 ± 0.01	
10	1.31 ± 0.01	1.37 ± 0.01	1.40 ± 0.01	1.38 ± 0.03	1.40 ± 0.00			
11	1.35 ± 0.01	1.40 ± 0.01	1.43 ± 0.01	1.38 ± 0.02				

The relative contributions and absolute concentrations of organics, nitrate, sulphate, ammonia, chloride and MSA are illustrated in Fig. S7 (SI) for experiments performed at 273 and 293 K. Absolute concentrations show that in general the aerosol mass loading was small and that the organic contribution was comparable during all experiments. As previously discussed in Rosati et al. (2021a) and Wollesen de Jonge et al. (2021) we cannot conclude on the exact origin of the organic signal. It cannot be entirely excluded that it is due to contamination from previous experiments. Since we do not know the type of organic it is difficult to access its potential impact on hygroscopicity. It could however also derive from biases due to the complex fragmentation during ionization, uncertainties arising from the calibration with MSA and previously documented memory effects

(e.g. Drewnick et al., 2009, 2015; Pieber et al., 2016). If this is the case, the organic signal will not influence hygroscopicity. The chemical composition of the aerosol particles could not be measured at 258 K due to the low mass produced during these experiments. Exp. 8 and 9 were carried out at 273 K but no obvious difference is found compared to the experiments carried out at 293 K. Figure 5 illustrates mean κ-values colour coded by the MSA to sulphate ratio measured by the HR-ToF-AMS at 293 and 273 K. We selected κ-values for dry particles of 80 and 100 nm (long-HTDMA) as these sizes are more representative of the size range analysed by the HR-ToF-AMS (typically PM_1). Tabular values of MSA/SO_4^{2-} are given in Table S5 in the SI. The MSA/SO_4^{2-} ratio is highest in Exp. 1 and 7, that were performed at 293 K and dry conditions, reaching values above 3. These high values at dry and warm conditions were already discussed in Wollesen de Jonge et al. (2021). Exp. 6, which was also carried out at 293 K and dry conditions, shows on the contrary a small MSA/SO_4^{2-} ratio of 1.3. This difference could potentially originate from the higher RH values of 13.7 ± 1.7 in Exp. 6 compared to RH below 10 % in Exp. 1 and 7. At 293 K and high humidity conditions the MSA/SO_4^{2-} ratios vary from 2.7 to 1.4, where experiments at low H_2O_2 concentrations yield high values and experiments at high H_2O_2 conditions yield low values. At 273 K and high humidity conditions the values during experiments with high or low H_2O_2 coincide yielding ratios of 1.5. As seen in Fig. 5 the κ-values at 273 K vary most, while their MSA/SO_4^{2-} ratios are the same. At 293 K, on the other hand, the MSA/SO_4^{2-} ratios vary from 3 to 1.4 as discussed above but no clear trend is observed in the κ-values, i.e. higher κ-values are both associated with high and low MSA/SO_4^{2-} ratios.

To the best of our knowledge there are no previous measurements of the water uptake of MSA or ammonium-MSA particles at 258 or 273 K. When using the UManSysProp thermodynamic model to calculate κ-values for ammonium sulphate particles at 293 and 258 K only small variations are found. κ-values of 0.59 and 0.58 at 293 and 258 K, respectively, are found based on hygroscopic growth, while κ-values of 0.63 and 0.59 at 293 and 258 K, respectively, are found based on CCN activation potential. This is consistent with previous findings showing that the water activity of ammonium sulphate in this temperature range is quite constant (Gysel et al., 2002). Due to the similarities between ammonium sulphate and MSA we thus expect that the temperature dependence of the water uptake of MSA is also negligible.

3.3 Quantum Chemical Calculations of Gas-phase Hydration of MSA

Gas-phase chemistry might be influenced by the presence of water molecules. We carried out detailed quantum chemical calculations to investigate whether the formed MSA is hydrated in the gas-phase. Figure 6 presents the lowest free energy cluster structures (298.15 K and 1 atm) obtained at the ωB97X-D/6-31++G(d,p) level of theory.

The formed $(MSA)_1(H_2O)_{1-5}$ clusters show some differences compared to the corresponding sulphuric acid - water clusters (see table S6). A proton transfer in the global free energy structures of the $(MSA)_1(H_2O)_{3-5}$ clusters is observed, whereas at least six water molecules are required in the case of sulphuric acid clusters (Kildgaard et al., 2018a). The calculated reaction free energy, at the DLPNO-CCSD(T_0)/aug-cc-pVTZ//ωB97X-D/6-31++G(d,p) level of theory, for adding the first four water molecules to MSA is less favourable than adding water molecules to sulfuric acid (see SI). This indicates that gas-phase MSA is significantly less hygroscopic compared to SA.

17
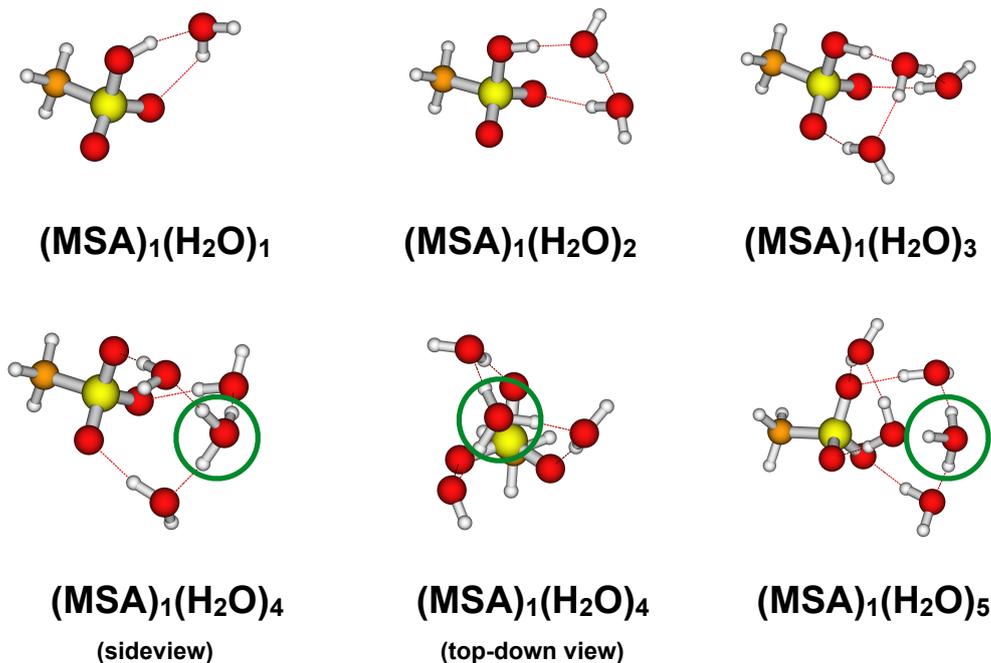
Figure 6. Identified lowest Gibbs free energy $(MSA)_1(H_2O)_{1-5}$ cluster structures calculated at the ωB97X-D/6-31++G(d,p) level of theory. The green circles indicate the formation of a H_3O^+ ion.

The hydrate distribution (x_n) of the $(MSA)_1(H_2O)_{1-5}$ clusters can be calculated to elucidate the extent to which the clusters are hydrated under realistic atmospheric conditions. The hydrate distributions can be calculated as follows (Henschel et al., 2014a):

$$x_n = \left(\frac{p(H_2O)}{p_{\text{ref}}} \right)^n x_0 \exp\left(-\frac{\Delta G_n}{RT} \right). \tag{7}$$

425　Here n is the given hydrate, ΔG_n is the binding free energy of the cluster and p_{ref} is the reference pressure (1 atm). The population of the unhydrated cluster x_0 is normalised so that all the populations sum up to 1. $p(H_2O) = 0.0316$ atm is the saturation water vapour pressure at 298.15 K. We find that the MSA clusters are predominantly not hydrated in the gas-phase (see Figure S10 in SI). At low RH (20%) the MSA monohydrate population is only 3%. At increasing RH the monohydrate becomes more pronounced, with a value of 14% at 100% RH. Even at 100% RH the dihydrate is only 0.7% populated. In

430　contrast, the monohydrate and dihydrate of SA is populated by 32% and 6%, respectively, at 100% RH (Kildgaard et al., 2018a). These findings imply that MSA is not significantly hydrated in the gas-phase and water should have little influence on the gas-phase chemistry. This is consistent with a previous study on the effect of a single water molecule on the reactions between the OH radical and MSA (Jörgensen et al., 2013), where water was also found to have no influence on the reaction kinetics.

4 Conclusions

The oceans emit large quantities of DMS, which can act as a precursor for the production and growth of aerosol particles. In this study we investigate the oxidation of DMS by hydroxyl radicals with a special focus on the hygroscopicity and CCN activity potential of the particles. The experiments were carried out in the temperature range 258 to 293 K at dry and humid conditions in the AURA chamber and complemented by quantum chemical calculations.

The nucleation and growth rates of the new particles formed were smaller at cold temperatures compared to at warm temperatures. This temperature dependence is unexpected but most likely originates from a slower oxidation of DMS at 258 K compared to at 293 K. Higher relative humidities did not seem to significantly affect the decay of DMS during oxidation with OH radicals but led to lower particle growth rates compared to at low relative humidities. Quantum chemical calculations revealed that gas-phase MSA clusters are predominantly not hydrated and thus high humidity conditions are not expected to influence its gas-phase chemistry.

The average hygroscopicity parameters, κ, calculated from measurements performed during the main particles' growth mode at sub- and supersaturated water vapour conditions at 293 K, ranged from 0.48 to 0.52 for dry 80 nm particles. These values are well comparable with modelled values for MSA or mixtures of MSA and ammonium sulphate (Fossum et al., 2018). These results are also consistent with online chemical composition measurements revealing that the largest fraction of the particles was MSA followed by ammonium sulphate. During ageing by exposure to hydroxyl radicals the water uptake of the particles increased, as found for all investigated sizes (D_{dry}=10 - 150 nm) at sub- and supersaturated water vapour conditions. The size selected results from the HR-ToF-AMS indicate that this could originate from a change in the MSA/sulphate ratio with ageing favouring more ammonium sulphate in the particles with longer ageing. When oxidising DMS at colder temperatures, a slight increase in κ-values is visible, which is more pronounced for smaller particles. The MSA/sulphate ratio did not show a clear temperature trend but showed a dependency on RH, where highest values were measured at low relative humidities.

The κ-values found in this study for particles produced by the oxidation of DMS by OH radicals lie within the upper range of the so-called "more-hygroscopic particle" (MHP) mode defined as κ range between approximately 0.17 and 0.66 by Swietlicki et al. (2008). This is the prevailing hygroscopicity group found from observations in the marine environment. Swietlicki et al. (2008) described a potential source of these particles to be partly neutralised DMS-derived sulphate particles as well as aged sea salt particles and mixtures with organic matter. Our hygroscopicity results are consistent with these observations underlining the high water uptake potential of particles formed via the oxidation of DMS by OH radicals. Aerosol particles from new particle formation have been shown to contribute the major fraction of all particles in remote continental regions (Spracklen et al., 2006). Specifically at Arctic sites new particles formed from the oxidation of DMS have been found to be important for the particle population, for their growth and for their potential to act as CCN (Beck et al., 2021; Schmale and Baccarini, 2021). Recently, Zheng et al. (2021) provided evidence for regular and frequent new particle formation in remote marine locations thereby contradicting the common view of rare occurrences in these areas (e.g. Kerminen et al., 2018). There is still a substantial knowledge gap of the detailed processes occurring in the ambient atmosphere. Thus, this laboratory study provides

new insights into the properties of particles formed from DMS oxidation at different temperatures and humidity regimes, which is needed to understand atmospheric observations.

References

485   Albu, M., Barnes, I., Becker, K. H., Patroescu-Klotz, I., Mocanu, R., and Benter, T.: Rate coefficients for the gas-phase reaction of OH radicals with dimethyl sulfide: temperature and O2 partial pressure dependence, Phys. Chem. Chem. Phys., 8, 728–736, https://doi.org/10.1039/B512536G, http://dx.doi.org/10.1039/B512536G, 2006.

Andreae, M. O.: Ocean–atmosphere Interactions in the Global Biogeochemical Sulfur Cycle, Marine Chem., 30, 1–29, 1990.

Ayers, G. P. and Cainey, J. M.: The CLAW hypothesis: a review of the major developments, Environmental Chemistry, 4, 366–374, 2007.

490   Barnes, I., Hjorth, J., and Mihalopoulos, N.: Dimethyl Sulfide and Dimethyl Sulfoxide and Their Oxidation in the Atmosphere, Chemical Reviews, 106, 940–975, https://doi.org/10.1021/cr020529+, https://doi.org/10.1021/cr020529+, 2006.

Beck, L. J., Sarnela, N., Junninen, H., Hoppe, C. J. M., Garmash, O., Bianchi, F., Riva, M., Rose, C., Peräkylä, O., Wimmer, D., Kausiala, O., Jokinen, T., Ahonen, L., Mikkilä, J., Hakala, J., He, X.-C., Kontkanen, J., Wolf, K. K. E., Cappelletti, D., Mazzola, M., Traversi, R., Petroselli, C., Viola, A. P., Vitale, V., Lange, R., Massling, A., Nøjgaard, J. K., Krejci, R., Karlsson, L., Zieger, P., Jang, S., Lee, K., Vakkari,
495   V., Lampilahti, J., Thakur, R. C., Leino, K., Kangasluoma, J., Duplissy, E.-M., Siivola, E., Marbouti, M., Tham, Y. J., Saiz-Lopez, A., Petäjä, T., Ehn, M., Worsnop, D. R., Skov, H., Kulmala, M., Kerminen, V.-M., and Sipilä, M.: Differing Mechanisms of New Particle Formation at Two Arctic Sites, Geophysical Research Letters, 48, e2020GL091 334, https://doi.org/https://doi.org/10.1029/2020GL091334, https://agupubs.onlinelibrary.wiley.com/doi/abs/10.1029/2020GL091334, e2020GL091334 2020GL091334, 2021.

Berg, O. H., Swietlicki, E., and Krejci, R.: Hygroscopic growth of aerosol particles in the marine boundary layer over the Pacific and Southern
500   Oceans during the First Aerosol Characterization Experiment (ACE 1), Journal of Geophysical Research: Atmospheres, 103, 16 535–16 545, https://doi.org/https://doi.org/10.1029/97JD02851, https://agupubs.onlinelibrary.wiley.com/doi/abs/10.1029/97JD02851, 1998.

Cappellin, L., Karl, T., Probst, M., Ismailova, O., Winkler, P. M., Soukoulis, C., Aprea, E., Märk, T. D., Gasperi, F., and Biasioli, F.: On Quantitative Determination of Volatile Organic Compound Concentrations Using Proton Transfer Reaction Time-of-Flight Mass Spectrometry, Environmental Science & Technology, 46, 2283–2290, https://doi.org/10.1021/es203985t, https://doi.org/10.1021/es203985t, 2012.

505   Carpenter, L. J., Archer, S. D., and Beale, R.: Ocean-atmosphere trace gas exchange, Chem. Soc. Rev., 41, 6473–6506, https://doi.org/10.1039/C2CS35121H, http://dx.doi.org/10.1039/C2CS35121H, 2012.

Chai, J.-D. and Head-Gordon, M.: Long-range Corrected Hybrid Density Functionals with Damped Atom-atom Dispersion Corrections, Phys. Chem. Chem. Phys., 10, 6615–6620, 2008.

Charlson, R. J., Lovelock, J. E., Andreae, M. O., and Warren, S. G.: Oceanic phytoplankton, atmospheric sulphur, cloud albedo and climate,
510   Nature, 326, 655–661, https://doi.org/10.1038/326655a0, http://www.nature.com/doifinder/10.1038/326655a0, 1987.

Collins, D. B., Ault, A. P., Moffet, R. C., Ruppel, M. J., Cuadra-Rodriguez, L. A., Guasco, T. L., Corrigan, C. E., Pedler, B. E., Azam, F., Aluwihare, L. I., Bertram, T. H., Roberts, G. C., Grassian, V. H., and Prather, K. A.: Impact of marine biogeochemistry on the chemical mixing state and cloud forming ability of nascent sea spray aerosol, Journal of Geophysical Research: Atmospheres, 118, 8553–8565, https://doi.org/https://doi.org/10.1002/jgrd.50598, https://agupubs.onlinelibrary.wiley.com/doi/abs/10.1002/jgrd.50598, 2013.

515   Collins, D. B., Bertram, T. H., Sultana, C. M., Lee, C., Axson, J. L., and Prather, K. A.: Phytoplankton blooms weakly influence the cloud forming ability of sea spray aerosol, Geophysical Research Letters, 43, 9975–9983, https://doi.org/https://doi.org/10.1002/2016GL069922, https://agupubs.onlinelibrary.wiley.com/doi/abs/10.1002/2016GL069922, 2016.

Covert, D. S., Gras, J. L., Wiedensohler, A., and Stratmann, F.: Comparison of directly measured CCN with CCN modeled from the number-size distribution in the marine boundary layer during ACE 1 at Cape Grim, Tasmania, Journal of Geophysical Research: Atmospheres, 103,

520 16 597–16 608, https://doi.org/https://doi.org/10.1029/98JD01093, https://agupubs.onlinelibrary.wiley.com/doi/abs/10.1029/98JD01093, 1998.

DeCarlo, P. F., Slowik, J. G., Worsnop, D. R., Davidovits, P., and Jimenez, J. L.: Particle Morphology and Density Characterization by Combined Mobility and Aerodynamic Diameter Measurements. Part 1: Theory, Aerosol Science and Technology, 38, 1185–1205, https://doi.org/10.1080/027868290903907, https://doi.org/10.1080/027868290903907, 2004.

525 Decarlo, P. F., Kimmel, J. R., Trimborn, A., Northway, M. J., Jayne, J. T., Aiken, A. C., Gonin, M., Fuhrer, K., Horvath, T., Docherty, K. S., Worsnop, D. R., and Jimenez, J. L.: Field-Deployable, High-Resolution, Time-of-Flight Aerosol Mass Spectrometer, Analytical Chemistry, 78, 8281–8289, https://doi.org/8410.1029/2001JD001213.Analytical, http://www.agu.org/pubs/crossref/2003/2001JD001213.shtml, 2006.

Ditas, F., Shaw, R. A., Siebert, H., Simmel, M., Wehner, B., and Wiedensohler, A.: Aerosols-cloud microphysics-thermodynamics-530 turbulence: evaluating supersaturation in a marine stratocumulus cloud, Atmospheric Chemistry and Physics, 12, 2459–2468, https://doi.org/10.5194/acp-12-2459-2012, https://acp.copernicus.org/articles/12/2459/2012/, 2012.

Drewnick, F., Hings, S. S., Alfarra, M. R., Prevot, A. S. H., and Borrmann, S.: Aerosol quantification with the Aerodyne Aerosol Mass Spectrometer: detection limits and ionizer background effects, Atmospheric Measurement Techniques, 2, 33–46, https://doi.org/10.5194/amt-2-33-2009, https://amt.copernicus.org/articles/2/33/2009/, 2009.

535 Drewnick, F., Diesch, J. M., Faber, P., and Borrmann, S.: Aerosol mass spectrometry: Particle-vaporizer interactions and their consequences for the measurements, Atmospheric Measurement Techniques, 8, 3811–3830, https://doi.org/10.5194/amt-8-3811-2015, 2015.

Duplissy, J., Merikanto, J., Franchin, A., Tsagkogeorgas, G., Kangasluoma, J., Wimmer, D., Vuollekoski, H., Schobesberger, S., Lehtipalo, K., Flagan, R. C., Brus, D., Donahue, N. M., Vehkamäki, H., Almeida, J., Amorim, A., Barmet, P., Bianchi, F., Breitenlechner, M., Dunne, E. M., Guida, R., Henschel, H., Junninen, H., Kirkby, J., Kürten, A., Kupc, A., Määttänen, A., Makhmutov, V., Mathot, S., Nieminen, 540 T., Onnela, A., Praplan, A. P., Riccobono, F., Rondo, L., Steiner, G., Tome, A., Walther, H., Baltensperger, U., Carslaw, K. S., Dommen, J., Hansel, A., Petäjä, T., Sipilä, M., Stratmann, F., Vrtala, A., Wagner, P. E., Worsnop, D. R., Curtius, J., and Kulmala, M.: Effect of ions on sulfuric acid-water binary particle formation: 2. Experimental data and comparison with QC-normalized classical nucleation theory, Journal of Geophysical Research: Atmospheres, 121, 1752–1775, https://doi.org/https://doi.org/10.1002/2015JD023539, https://agupubs.onlinelibrary.wiley.com/doi/abs/10.1002/2015JD023539, 2016.

545 Elm, J. and Kristensen, K.: Basis Set Convergence of the Binding Energies of Strongly Hydrogen-Bonded Atmospheric Clusters, Phys. Chem. Chem. Phys, 19, 1122–1133, 2017.

Elm, J. and Mikkelsen, K. V.: Computational Approaches for Efficiently Modelling of Small Atmospheric Clusters, Chem. Phys. Lett., 615, 26–29, 2014.

Elm, J., Bilde, M., and Mikkelsen, K. V.: Assessment of Binding Energies of Atmopsheric Clusters, Phys. Chem. Chem. Phys, 15, 16 442–550 16 445, 2013.

Facchini, M., Rinaldi, M., Decesari, S., Carbone, C., Finessi, E., Mircea, M., Fuzzi, S., Ceburnis, D., Flanagan, R., Nilsson, E., de Leeuw, G., Martino, M., Woeltjen, J., and O'Dowd, C.: Primary submicron marine aerosol dominated by insoluble organic colloids and aggregates, Geophysical Research Letters, 35, 1–5, https://doi.org/10.1029/2008GL034210, https://www.scopus.com/inward/record.uri?eid=2-s2.0-55449122901&doi=10.1029%2f2008GL034210&partnerID=40&md5=fd0b15ec59472f2e28c838cdfd84177f, 2008.

555 Fossum, K. N., Ovadnevaite, J., Ceburnis, D., Dall'Osto, M., Marullo, S., Bellacicco, M., Simó, R., Liu, D., Flynn, M., Zuend, A., et al.: Summertime primary and secondary contributions to Southern Ocean cloud condensation nuclei, Scientific reports, 8, 1–14, 2018.

Frisch, M., Trucks, G. W., Schlegel, H. B., Scuseria, G. E., Robb, M. A., Cheeseman, J. R., Scalmani, G., Barone, V., Mennucci, B., Petersson, G. A., et al., and Gaussian, Inc., W. C.: Gaussian 09, 2013.

Fuentes, E., Coe, H., Green, D., and McFiggans, G.: On the impacts of phytoplankton-derived organic matter on the properties of the primary marine aerosol Part 2: Composition, hygroscopicity and cloud condensation activity, Atmospheric Chemistry and Physics, 11, 2585–2602, https://doi.org/10.5194/acp-11-2585-2011, https://www.atmos-chem-phys.net/11/2585/2011/, 2011.

Graus, M., Müller, M., and Hansel, A.: High Resolution PTR-TOF: Quantification and Formula Confirmation of VOC in Real Time, Journal of the American Society for Mass Spectrometry, 21, 1037–1044, https://doi.org/https://doi.org/10.1016/j.jasms.2010.02.006, https://www.sciencedirect.com/science/article/pii/S1044030510001005, 2010.

Gysel, M., Weingartner, E., and Baltensperger, U.: Hygroscopicity of Aerosol Particles at Low Temperatures. 2. Theoretical and Experimental Hygroscopic Properties of Laboratory Generated Aerosols, Environmental Science & Technology, 36, 63–68, https://doi.org/10.1021/es010055g, https://doi.org/10.1021/es010055g, 2002.

Henschel, H., Navarro, J. C. A., Yli-Juuti, T., Kupiainen-Määttä, O., Olenius, T., Ortega, I. K., Clegg, S. L., Kurtén, T., Riipinen, I., and Vehkamäki, H.: Hydration of Atmospherically Relevant Molecular Clusters: Computational Chemistry and Classical Thermodynamics, J. Phys. Chem. A., 118, 2599–2611, 2014a.

Henschel, H., Navarro, J. C. A., Yli-Juuti, T., Kupiainen-Määttä, O., Olenius, T., Ortega, I. K., Clegg, S. L., Kurtén, T., Riipinen, I., and Vehkamäki, H.: Hydration of Atmospherically Relevant Molecular Clusters: Computational Chemistry and Classical Thermodynamics, The Journal of Physical Chemistry A, 118, 2599–2611, https://doi.org/10.1021/jp500712y, https://doi.org/10.1021/jp500712y, pMID: 24678924, 2014b.

Henschel, H., Kurtén, T., and Vehkamäki, H.: Computational Study on the Effect of Hydration on New Particle Formation in the Sulfuric Acid/Ammonia and Sulfuric Acid/ Dimethylamine Systems, J. Phys. Chem. A., 120, 1886–1896, 2016.

Hoffmann, E. H., Tilgner, A., Schrödner, R., Bräuer, P., Wolke, R., and Herrmann, H.: An advanced modeling study on the impacts and atmospheric implications of multiphase dimethyl sulfide chemistry, Proceedings of the National Academy of Sciences, 113, 11 776–11 781, https://doi.org/10.1073/pnas.1606320113, https://www.pnas.org/content/113/42/11776, 2016.

Hopkins, F. E., Bell, T. G., Yang, M., Suggett, D. J., and Steinke, M.: Air exposure of coral is a significant source of dimethylsulfide (DMS) to the atmosphere, Scientific Reports, 6, 1–11, 2016.

IPCC: Climate Change 2021: The Physical Science Basis. Contribution of Working Group I to the Sixth Assessment Report of the Intergovernmental Panel on Climate Change, Cambridge University Press, Cambridge, United Kingdom and New York, NY, USA, masson-Delmotte, V., P. Zhai, A. Pirani, S.L. Connors, C. Péan, S. Berger, N. Caud, Y. Chen, L. Goldfarb, M.I. Gomis, M. Huang, K. Leitzell, E. Lonnoy, J.B.R. Matthews, T.K. Maycock, T. Waterfield, O. Yelekçi, R. Yu, and B. Zhou (eds.), 2021.

Johnson, G., Ristovski, Z., and Morawska, L.: Method for measuring the hygroscopic behaviour of lower volatility fractions in an internally mixed aerosol, Journal of Aerosol Science, 35, 443–455, https://doi.org/https://doi.org/10.1016/j.jaerosci.2003.10.008, https://www.sciencedirect.com/science/article/pii/S0021850203004464, 2004.

Jörgensen, S., Jensen, C., Kjaergaard, H. G., and Anglada, J. M.: The Gas-phase Reaction of Methane Sulfonic Acid with the Hydroxyl Radical Without and With Water Vapor, Phys. Chem. Chem. Phys., 15, 5140–5150, 2013.

Kerminen, V.-M., Chen, X., Vakkari, V., Petäjä, T., Kulmala, M., and Bianchi, F.: Atmospheric new particle formation and growth: review of field observations, Environmental Research Letters, 13, 103 003, https://doi.org/10.1088/1748-9326/aadf3c, https://doi.org/10.1088/1748-9326/aadf3c, 2018.

23

Keskinen, H., Romakkaniemi, S., Jaatinen, A., Miettinen, P., Saukko, E., Jorma, J., Mäkelä, J. M., Virtanen, A., Smith, J. N., and Laaksonen, A.: On-Line Characterization of Morphology and Water Adsorption on Fumed Silica Nanoparticles, Aerosol Science and Technology, 45, 1441–1447, https://doi.org/10.1080/02786826.2011.597459, https://doi.org/10.1080/02786826.2011.597459, 2011.

Kildgaard, J. V., Mikkelsen, K. V., Bilde, M., and Elm, J.: Hydration of Atmospheric Molecular Clusters: A New Method for Systematic Configurational Sampling, J. Phys. Chem. A, 122, 5026–5036, 2018a.

Kildgaard, J. V., Mikkelsen, K. V., Bilde, M., and Elm, J.: Hydration of Atmospheric Molecular Clusters II: Organic Acid-Water Clusters, J. Phys. Chem. A, 122, 8549–8556, 2018b.

King, S., Butcher, A., Rosenoern, T., Coz, E., Lieke, K., De Leeuw, G., Nilsson, E., and Bilde, M.: Investigating primary marine aerosol properties: CCN activity of sea salt and mixed inorganic-organic particles, Environmental Science and Technology, 46, 10 405–10 412, https://doi.org/10.1021/es300574u, https://www.scopus.com/inward/record.uri?eid=2-s2.0-84867055687&doi=10.1021%2fes300574u&partnerID=40&md5=0c579e9c6bb0b2f4778b0cd06e6b0dd7, 2012.

Kristensen, K., Jensen, L., Glasius, M., and Bilde, M.: The effect of sub-zero temperature on the formation and composition of secondary organic aerosol from ozonolysis of alpha-pinene, Environmental Science: Processes and Impacts, 19, 1220–1234, https://doi.org/10.1039/c7em00231a, https://www.scopus.com/inward/record.uri?eid=2-s2.0-85031813918&doi=10.1039%2fc7em00231a&partnerID=40&md5=e22522820fdd3708111a7b0755ee7198, 2017.

Kulmala, M., Petäjä, T., Nieminen, T., Sipilä, M., Manninen, H., Lehtipalo, K., Dal Maso, M., Aalto, P., Junninen, H., Paasonen, P., Riipinen, I., Lehtinen, K., Laaksonen, A., and Kerminen, V.-M.: Measurement of the nucleation of atmospheric aerosol particles, Nature Protocols, 7, 1651–1667, https://doi.org/10.1038/nprot.2012.091, https://www.scopus.com/inward/record.uri?eid=2-s2.0-84866072109&doi=10.1038%2fnprot.2012.091&partnerID=40&md5=b211d1302a986e7582c4c47d76cfbdb2, 2012.

Kulmala, M., Kontkanen, J., Junninen, H., Lehtipalo, K., Manninen, H. E., Nieminen, T., Petäjä, T., Sipilä, M., Schobesberger, S., Rantala, P., and et al.: Direct Observations of Atmospheric Aerosol Nucleation, Science, 339, 943–946, 2013.

Lehtinen, K. E. J. and Kulmala, M.: A model for particle formation and growth in the atmosphere with molecular resolution in size, Atmospheric Chemistry and Physics, 3, 251–257, https://doi.org/10.5194/acp-3-251-2003, https://www.atmos-chem-phys.net/3/251/2003/, 2003.

Leverentz, H. R., Siepmann, J. I., Truhlar, D. G., Loukonen, V., and Vehkamäki, H.: Energetics of Atmospherically Implicated Clusters Made of Sulfuric Acid, Ammonia, and Dimethyl Amine, J. Phys. Chem. A, 117, 3819–3825, 2013.

Lewis, E. and Schwartz, S.: Sea Salt Aerosol Production: Mechanisms, Methods, Measurements and Models, American Geophysical Union, Washington DC, 2004.

Li, M., Karu, E., Brenninkmeijer, C., Fischer, H., Lelieveld, J., and Williams, J.: Tropospheric OH and stratospheric OH and Cl concentrations determined from CH_4, CH_3Cl, and SF_6 measurements, NPJ Climate and Atmospheric Science, 1, 1–7, 2018.

Liu, D., Nyord, T., Rong, L., and Feilberg, A.: Real-time quantification of emissions of volatile organic compounds from land spreading of pig slurry measured by PTR-MS and wind tunnels, Science of The Total Environment, 639, 1079 – 1087, https://doi.org/https://doi.org/10.1016/j.scitotenv.2018.05.149, http://www.sciencedirect.com/science/article/pii/S0048969718317972, 2018.

Lopez-Yglesias, X. F., Yeung, M. C., Dey, S. E., Brechtel, F. J., and Chan, C. K.: Performance Evaluation of the Brechtel Mfg. Humidified Tandem Differential Mobility Analyzer (BMI HTDMA) for Studying Hygroscopic Properties of Aerosol Particles, Aerosol Science and Technology, 48, 969–980, https://doi.org/10.1080/02786826.2014.952366, https://doi.org/10.1080/02786826.2014.952366, 2014.

Manninen, H. E., Nieminen, T., Asmi, E., Gagné, S., Häkkinen, S., Lehtipalo, K., Aalto, P., Vana, M., Mirme, A., Mirme, S., Hõrrak, U., Plass-Dülmer, C., Stange, G., Kiss, G., Hoffer, A., TörÅ', N., Moerman, M., Henzing, B., de Leeuw, G., Brinkenberg, M., Kouvarakis, G. N., Bougiatioti, A., Mihalopoulos, N., O'Dowd, C., Ceburnis, D., Arneth, A., Svenningsson, B., Swietlicki, E., Tarozzi, L., Decesari, S., Facchini, M. C., Birmili, W., Sonntag, A., Wiedensohler, A., Boulon, J., Sellegri, K., Laj, P., Gysel, M., Bukowiecki, N., Weingartner, E., Wehrle, G., Laaksonen, A., Hamed, A., Joutsensaari, J., Petäjä, T., Kerminen, V.-M., and Kulmala, M.: EUCAARI ion spectrometer measurements at 12 European sites – analysis of new particle formation events, Atmospheric Chemistry and Physics, 10, 7907–7927, https://doi.org/10.5194/acp-10-7907-2010, https://www.atmos-chem-phys.net/10/7907/2010/, 2010.

Mardyukov, A. and Schreiner, P. R.: Atmospherically Relevant Radicals Derived from the Oxidation of Dimethyl Sulfide, Acc. Chem. Res., 51, 475–483, 2018.

Modini, R. L., Johnson, G. R., He, C., and Ristovski, Z. D.: Observation of the suppression of water uptake by marine particles, Atmospheric Research, 98, 219–228, https://doi.org/https://doi.org/10.1016/j.atmosres.2010.03.025, https://www.sciencedirect.com/science/article/pii/S0169809510000748, international Conference on Nucleation and Atmospheric Aerosols (Part 1), 2010.

Moore, R. H., Nenes, A., and Medina, J.: Scanning Mobility CCN Analysis—A Method for Fast Measurements of Size-Resolved CCN Distributions and Activation Kinetics, Aerosol Science and Technology, 44, 861–871, https://doi.org/10.1080/02786826.2010.498715, 2010.

Myllys, N., Elm, J., and Kurtén, T.: Density Functional Theory Basis Set Convergence of Sulfuric Acid-Containing Molecular Clusters, Comp. Theor. Chem., 1098, 1–12, 2016.

Neese, F.: doi:10.1002/wcms.81, wIREs Comput Mol Sci 2012, 2: 73-78, 2012.

Nguyen, Q. T., Kjær, K. H., Kling, K. I., Boesen, T., and Bilde, M.: Impact of fatty acid coating on the CCN activity of sea salt particles, Tellus B: Chemical and Physical Meteorology, 69, 1304 064, https://doi.org/10.1080/16000889.2017.1304064, https://doi.org/10.1080/16000889.2017.1304064, 2017.

Nilsson, E. D., Rannik, U., Swietlicki, E., Leck, C., Aalto, P. P., Zhou, J., and Norman, M.: Turbulent aerosol fluxes over the Arctic Ocean: 2. Wind-driven sources from the sea, Journal of Geophysical Research: Atmospheres, 106, 32 139–32 154, https://doi.org/10.1029/2000JD900747, https://agupubs.onlinelibrary.wiley.com/doi/abs/10.1029/2000JD900747, 2001.

Ovadnevaite, J., Ceburnis, D., Martucci, G., Bialek, J., Monahan, C., Rinaldi, M., Facchini, M. C., Berresheim, H., Worsnop, D. R., and O'Dowd, C.: Primary marine organic aerosol: A dichotomy of low hygroscopicity and high CCN activity, Geophysical Research Letters, 38, https://doi.org/https://doi.org/10.1029/2011GL048869, https://agupubs.onlinelibrary.wiley.com/doi/abs/10.1029/2011GL048869, 2011.

Pajunoja, A., Lambe, A. T., Hakala, J., Rastak, N., Cummings, M. J., Brogan, J. F., Hao, L., Paramonov, M., Hong, J., Prisle, N. L., Malila, J., Romakkaniemi, S., Lehtinen, K. E. J., Laaksonen, A., Kulmala, M., Massoli, P., Onasch, T. B., Donahue, N. M., Riipinen, I., Davidovits, P., Worsnop, D. R., Petäjä, T., and Virtanen, A.: Adsorptive uptake of water by semisolid secondary organic aerosols, Geophysical Research Letters, 42, 3063–3068, https://doi.org/https://doi.org/10.1002/2015GL063142, https://agupubs.onlinelibrary.wiley.com/doi/abs/10.1002/2015GL063142, 2015.

Peng, C. and Chan, C. K.: The water cycles of water-soluble organic salts of atmospheric importance, Atmospheric Environment, 35, 1183–1192, https://doi.org/https://doi.org/10.1016/S1352-2310(00)00426-X, https://www.sciencedirect.com/science/article/pii/S135223100000426X, 2001.

Petters, M. D. and Kreidenweis, S. M.: A single parameter representation of hygroscopic growth and cloud condensation nucleus activity, Atmospheric Chemistry and Physics, 7, 1961–1971, https://doi.org/10.5194/acp-7-1961-2007, https://www.atmos-chem-phys.net/7/1961/2007/, 2007.

670   Pieber, S. M., El Haddad, I., Slowik, J. G., Canagaratna, M. R., Jayne, J. T., Platt, S. M., Bozzetti, C., Daellenbach, K. R., Fröhlich, R., Vlachou, A., Klein, F., Dommen, J., Miljevic, B., Jiménez, J. L., Worsnop, D. R., Baltensperger, U., and Prévôt, A. S. H.: Inorganic Salt Interference on CO_2+ in Aerodyne AMS and ACSM Organic Aerosol Composition Studies, Environmental Science & Technology, p. acs.est.6b01035, https://doi.org/10.1021/acs.est.6b01035, http://pubs.acs.org/doi/abs/10.1021/acs.est.6b01035, 2016.

Prather, K., Bertram, T., Grassian, V., Deane, G., Stokes, M., DeMott, P., Aluwihare, L., Palenik, B., Azam, F., Seinfeld, J., Mof-
675   fet, R., Molina, M., Cappa, C., Geiger, F., Roberts, G., Russell, L., Ault, A., Baltrusaitis, J., Collins, D., Corrigan, C., Cuadra-Rodriguez, L., Ebben, C., Forestieri, S., Guasco, T., Hersey, S., Kim, M., Lambert, W., Modini, R., Mui, W., Pedler, B., Ruppel, M., Ryder, O., Schoepp, N., Sullivan, R., and Zhao, D.: Bringing the ocean into the laboratory to probe the chemical complexity of sea spray aerosol, Proceedings of the National Academy of Sciences of the United States of America, 110, 7550–7555, https://doi.org/10.1073/pnas.1300262110, https://www.scopus.com/inward/record.uri?eid=2-s2.0-84877322862&doi=
680   10.1073%2fpnas.1300262110&partnerID=40&md5=dfd88be94b5eee439d2522f8d3ffada7, 2013.

Quinn, P. and Bates, T.: The case against climate regulation via oceanic phytoplankton sulphur emissions, Nature, 480, 51–6, https://doi.org/10.1038/nature10580, 2011.

Rastak, N., Pajunoja, A., Acosta Navarro, J. C., Ma, J., Song, M., Partridge, D. G., Kirkevåg, A., Leong, Y., Hu, W. W., Taylor, N. F., Lambe, A., Cerully, K., Bougiatioti, A., Liu, P., Krejci, R., Petäjä, T., Percival, C., Davidovits, P., Worsnop, D. R., Ekman, A. M. L., Nenes, A., Mar-
685   tin, S., Jimenez, J. L., Collins, D. R., Topping, D., Bertram, A. K., Zuend, A., Virtanen, A., and Riipinen, I.: Microphysical explanation of the RH-dependent water affinity of biogenic organic aerosol and its importance for climate, Geophysical Research Letters, 44, 5167–5177, https://doi.org/https://doi.org/10.1002/2017GL073056, https://agupubs.onlinelibrary.wiley.com/doi/abs/10.1002/2017GL073056, 2017.

Riplinger, C. and Neese, F.: An Efficient and Near Linear Scaling Pair Natural Orbital Based Local Coupled Cluster Method, J. Chem. Phys., 138, 034 106, 2013.

690   Riplinger, C., Sandhoefer, B., Hansen, A., and Neese, F.: Natural Triple Excitations in Local Coupled Cluster Calculations with Pair Natural Orbitals, J. Chem. Phys., 139, 134 101, 2013.

Roberts, G. C. and Nenes, A.: A Continuous-Flow Streamwise Thermal-Gradient CCN Chamber for Atmospheric Measurements, Aerosol Science and Technology, 39, 206–221, https://doi.org/10.1080/027868290913988, 2005.

Rosati, B., Paul, A., Iversen, E. M., Massling, A., and Bilde, M.: Reconciling atmospheric water uptake by hydrate forming salts, Environ.
695   Sci.: Processes Impacts, 22, 1759–1767, https://doi.org/10.1039/D0EM00179A, http://dx.doi.org/10.1039/D0EM00179A, 2020.

Rosati, B., Christiansen, S., Wollesen de Jonge, R., Roldin, P., Jensen, M. M., Wang, K., Moosakutty, S. P., Thomsen, D., Salomonsen, C., Hyttinen, N., Elm, J., Feilberg, A., Glasius, M., and Bilde, M.: New Particle Formation and Growth from Dimethyl Sulfide Oxidation by Hydroxyl Radicals, ACS Earth and Space Chemistry, 5, 801–811, https://doi.org/10.1021/acsearthspacechem.0c00333, https://doi.org/10.1021/acsearthspacechem.0c00333, 2021a.

700   Rosati, B., Christiansen, S., Dinesen, A., Roldin, P., Massling, A., E, D. N., and Bilde, M.: The impact of atmospheric oxidation on hygroscopicity and cloud droplet activation of inorganic sea spray aerosol, Scientific Reports, 11, 10 008, https://doi.org/10.1038/s41598-021-89346-6, 2021b.

Schmale, J. and Baccarini, A.: Progress in Unraveling Atmospheric New Particle Formation and Growth Across the Arctic, Geophysical Research Letters, 48, e2021GL094 198, https://doi.org/https://doi.org/10.1029/2021GL094198, https://agupubs.onlinelibrary.wiley.com/doi/abs/10.1029/2021GL094198, e2021GL094198 2021GL094198, 2021.

Schmitz, G. and Elm, J.: Assessment of the DLPNO binding energies of strongly non-covalent bonded atmospheric molecular clusters, ACS Omega, 5, 7601–7612, 2020.

Seinfeld, J. and Pandis, S.: Atmospheric Chemistry and Physics: From Air Pollution to Climate Change, 3rd Edition, Wiley & Sons, Inc., 2016.

Sekimoto, K., Li, S.-M., Yuan, B., Koss, A., Coggon, M., Warneke, C., and de Gouw, J.: Calculation of the sensitivity of proton-transfer-reaction mass spectrometry (PTR-MS) for organic trace gases using molecular properties, International Journal of Mass Spectrometry, 421, 71 – 94, https://doi.org/https://doi.org/10.1016/j.ijms.2017.04.006, http://www.sciencedirect.com/science/article/pii/S1387380616302494, 2017.

Smith, M.: Sea-salt particles and the CLAW hypothesis, Environmental Chemistry, 4, 391–395, 2007.

Spracklen, D. V., Carslaw, K. S., Kulmala, M., Kerminen, V.-M., Mann, G. W., and Sihto, S.-L.: The contribution of boundary layer nucleation events to total particle concentrations on regional and global scales, Atmospheric Chemistry and Physics, 6, 5631–5648, https://doi.org/10.5194/acp-6-5631-2006, https://acp.copernicus.org/articles/6/5631/2006/, 2006.

Stewart, J. J. P.: Optimization of Parameters for Semiempirical Methods. V. Modification of NDDO Approximations and Application to 70 Elements, J. Molec. Modeling, 13, 1173–1213, 2007.

Swietlicki, E., Hansson, H.-C., Hämeri, K., Svenningsson, B., Massling, A., Mcfiggans, G., Mcmurry, P., Petäjä, T., Tunved, P., Gysel, M., Topping, D., Weingartner, E., Baltensperger, U., Rissler, J., Wiedensohler, A., and Kulmala, M.: Hygroscopic properties of submicrometer atmospheric aerosol particles measured with H-TDMA instruments in various environments - A review, Tellus, Series B: Chemical and Physical Meteorology, 60 B, 432–469, https://doi.org/10.1111/j.1600-0889.2008.00350.x, https://www.scopus.com/inward/record.uri?eid=2-s2.0-45449110434&doi=10.1111%2fj.1600-0889.2008.00350.x&partnerID=40&md5=1bed31a576a55599d9cb0c700a92d8a3, 2008.

Taipale, R., Ruuskanen, T. M., Rinne, J., Kajos, M. K., Hakola, H., Pohja, T., and Kulmala, M.: Technical Note: Quantitative long-term measurements of VOC concentrations by PTR-MS; measurement, calibration, and volume mixing ratio calculation methods, Atmospheric Chemistry and Physics, 8, 6681–6698, https://doi.org/10.5194/acp-8-6681-2008, https://www.atmos-chem-phys.net/8/6681/2008/, 2008.

Tang, M., Guo, L., Bai, Y., Huang, R.-J., Wu, Z., Wang, Z., Zhang, G., Ding, X., Hu, M., and Wang, X.: Impacts of methanesulfonate on the cloud condensation nucleation activity of sea salt aerosol, Atmospheric Environment, 201, 13–17, 2019.

Tikkanen, O.-P., Väisänen, O., Hao, L., Holopainen, E., Wang, H., Lehtinen, K. E. J., Virtanen, A., and Yli-Juuti, T.: Hygroscopicity of dimethylaminium-, sulfate-, and ammonium-containing nanoparticles, Aerosol Science and Technology, 52, 971–983, https://doi.org/10.1080/02786826.2018.1484071, https://doi.org/10.1080/02786826.2018.1484071, 2018.

Tomicic, M., Bødker Enghoff, M., and Svensmark, H.: Experimental study of H_2SO_4 aerosol nucleation at high ionization levels, Atmospheric Chemistry and Physics, 18, 5921–5930, https://doi.org/10.5194/acp-18-5921-2018, https://acp.copernicus.org/articles/18/5921/2018/, 2018.

Topping, D., Barley, M., Bane, M. K., Higham, N., Aumont, B., Dingle, N., and McFiggans, G.: UManSysProp v1.0: an online and open-source facility for molecular property prediction and atmospheric aerosol calculations, Geoscientific Model Development, 9, 899–914, https://doi.org/10.5194/gmd-9-899-2016, https://gmd.copernicus.org/articles/9/899/2016/, 2016.

Vallina, S. M. and Simó, R.: Re-visiting the CLAW hypothesis, Environmental Chemistry, 4, 384–387, 2007.

Vanhanen, J., Mikkilä, J., Lehtipalo, K., Sipilä, M., Manninen, H. E., Siivola, E., Petäjä, T., and Kulmala, M.: Particle Size Magnifier for Nano-CN Detection, Aerosol Science and Technology, 45, 533–542, https://doi.org/10.1080/02786826.2010.547889, https://www.tandfonline.com/doi/abs/10.1080/02786826.2010.547889, 2011.

Veres, P. R., Neuman, J. A., Bertram, T. H., Assaf, E., Wolfe, G. M., Williamson, C. J., Weinzierl, B., Tilmes, S., Thompson, C. R., Thames, A. B., Schroder, J. C., Saiz-Lopez, A., Rollins, A. W., Roberts, J. M., Price, D., Peischl, J., Nault, B. A., Møller, K. H., Miller, D. O., Meinardi, S., Li, Q., Lamarque, J.-F., Kupc, A., Kjaergaard, H. G., Kinnison, D., Jimenez, J. L., Jernigan, C. M., Hornbrook, R. S., Hills, A., Dollner, M., Day, D. A., Cuevas, C. A., Campuzano-Jost, P., Burkholder, J., Bui, T. P., Brune, W. H., Brown, S. S., Brock, C. A., Bourgeois, I., Blake, D. R., Apel, E. C., and Ryerson, T. B.: Global airborne sampling reveals a previously unobserved dimethyl sulfide oxidation mechanism in the marine atmosphere, Proceedings of the National Academy of Sciences, 117, 4505–4510, https://doi.org/10.1073/pnas.1919344117, https://www.pnas.org/content/117/9/4505, 2020.

Whitehead, J. D., Irwin, M., Allan, J. D., Good, N., and McFiggans, G.: A meta-analysis of particle water uptake reconciliation studies, Atmospheric Chemistry and Physics, 14, 11 833–11 841, https://doi.org/10.5194/acp-14-11833-2014, https://acp.copernicus.org/articles/14/11833/2014/, 2014.

Wollesen de Jonge, R., Elm, J., Rosati, B., Christiansen, S., Hyttinen, N., Lüdemann, D., Bilde, M., and Roldin, P.: Secondary aerosol formation from dimethyl sulfide – improved mechanistic understanding based on smog chamber experiments and modelling, Atmospheric Chemistry and Physics, 21, 9955–9976, https://doi.org/10.5194/acp-21-9955-2021, https://acp.copernicus.org/articles/21/9955/2021/, 2021.

Ye, Q., Goss, M. B., Isaacman-VanWertz, G., Zaytsev, A., Massoli, P., Lim, C., Croteau, P., Canagaratna, M., Knopf, D. A., Keutsch, F. N., Heald, C. L., and Kroll, J. H.: Organic Sulfur Products and Peroxy Radical Isomerization in the OH Oxidation of Dimethyl Sulfide, ACS Earth and Space Chemistry, 5, 2013–2020, https://doi.org/10.1021/acsearthspacechem.1c00108, https://doi.org/10.1021/acsearthspacechem.1c00108, 2021.

Yli-Juuti, T., Nieminen, T., Hirsikko, A., Aalto, P. P., Asmi, E., Hõrrak, U., Manninen, H. E., Patokoski, J., Dal Maso, M., Petäjä, T., Rinne, J., Kulmala, M., and Riipinen, I.: Growth rates of nucleation mode particles in Hyytiälä during 2003 – 2009: variation with particle size, season, data analysis method and ambient conditions, Atmospheric Chemistry and Physics, 11, 12 865–12 886, https://doi.org/10.5194/acp-11-12865-2011, https://www.atmos-chem-phys.net/11/12865/2011/, 2011.

Zhao, D. F., Buchholz, A., Kortner, B., Schlag, P., Rubach, F., Fuchs, H., Kiendler-Scharr, A., Tillmann, R., Wahner, A., Watne, Å. K., Hallquist, M., Flores, J. M., Rudich, Y., Kristensen, K., Hansen, A. M. K., Glasius, M., Kourtchev, I., Kalberer, M., and Mentel, T. F.: Cloud condensation nuclei activity, droplet growth kinetics, and hygroscopicity of biogenic and anthropogenic secondary organic aerosol (SOA), Atmospheric Chemistry and Physics, 16, 1105–1121, https://doi.org/10.5194/acp-16-1105-2016, https://acp.copernicus.org/articles/16/1105/2016/, 2016.

Zheng, G., Wang, Y., Wood, R., Jensen, M. P., Kuang, C., McCoy, I. L., Matthews, A., Mei, F., Tomlinson, J. M., Shilling, J. E., et al.: New particle formation in the remote marine boundary layer, Nature communications, 12, 1–10, 2021.

Zuend, A., Marcolli, C., Luo, B. P., and Peter, T.: A thermodynamic model of mixed organic-inorganic aerosols to predict activity coefficients, Atmospheric Chemistry and Physics, 8, 4559–4593, https://doi.org/10.5194/acp-8-4559-2008, https://acp.copernicus.org/articles/8/4559/2008/, 2008.

Zuend, A., Marcolli, C., Booth, A. M., Lienhard, D. M., Soonsin, V., Krieger, U. K., Topping, D. O., McFiggans, G., Peter, T., and Seinfeld, J. H.: New and extended parameterization of the thermodynamic model AIOMFAC: calculation of activity coefficients for organic-

inorganic mixtures containing carboxyl, hydroxyl, carbonyl, ether, ester, alkenyl, alkyl, and aromatic functional groups, Atmospheric Chemistry and Physics, 11, 9155–9206, https://doi.org/10.5194/acp-11-9155-2011, https://acp.copernicus.org/articles/11/9155/2011/, 2011.

780